



CERN-EP-2017-208
 LHCb-PAPER-2017-030
 26th March 2018

Measurement of CP observables in $B^\pm \rightarrow DK^{*\pm}$ decays using two- and four-body D final states

The LHCb collaboration[†]

Abstract

Measurements of CP observables in $B^\pm \rightarrow DK^{*\pm}$ decays are presented, where D denotes a superposition of D^0 and \bar{D}^0 meson states. Decays of the D meson to $K^-\pi^+$, K^-K^+ , $\pi^-\pi^+$, $K^-\pi^+\pi^-\pi^+$ and $\pi^-\pi^+\pi^-\pi^+$ are used and the $K^{*\pm}$ meson is reconstructed in the $K_S^0\pi^\pm$ final state. This analysis uses a data sample of pp collisions collected with the LHCb experiment, corresponding to integrated luminosities of 1 fb^{-1} , 2 fb^{-1} and 1.8 fb^{-1} at centre-of-mass energies $\sqrt{s} = 7\text{ TeV}$, 8 TeV and 13 TeV , respectively. The sensitivity of the results to the CKM angle γ is discussed.

Published in JHEP 11 (2017) 156

© CERN on behalf of the LHCb collaboration, licence CC-BY-4.0.

[†]Authors are listed at the end of this paper.

1 Introduction

A key characteristic of the Standard Model is that CP violation originates from a single phase in the CKM quark-mixing matrix [1, 2]. In the Standard Model the CKM matrix is unitary, leading to the condition $V_{ud}V_{ub}^* + V_{cd}V_{cb}^* + V_{td}V_{tb}^* = 0$, where V_{ij} are the CKM matrix elements. This relation is represented as a triangle in the complex plane, with angles α , β and γ , and an area proportional to the amount of CP violation in the quark sector of the Standard Model [3]. Overconstraining this unitarity triangle may lead to signs of physics beyond the Standard Model. The CKM angle $\gamma \equiv \arg\left(-\frac{V_{ud}V_{ub}^*}{V_{cd}V_{cb}^*}\right)$ is the least well-known angle of the CKM unitarity triangle. The latest published LHCb combination from direct measurements with charged and neutral B decays to a D meson (reconstructed in one of a variety of final states) and a kaon is $\gamma = (72.2_{-7.3}^{+6.8})^\circ$ [4]. A global fit to the CKM triangle by the CKMfitter group [5] obtains a γ value of $(66.9_{-3.4}^{+0.9})^\circ$, where this determination of γ excludes all direct measurements. The uncertainties on the indirect measurement are expected to decrease as lattice QCD calculations become more accurate. Therefore, precision at the level of 1° on a direct measurement of γ would test the consistency of the direct and indirect measurements and thereby the Standard Model. This precision can be achieved through a combination of measurements of various B decays that are sensitive to γ .

Direct measurements of γ can be made by exploiting the interference between $b \rightarrow c\bar{u}s$ and $b \rightarrow u\bar{c}s$ transitions. These transitions are present in $B \rightarrow D^{(*)}K^{(*)}$ decays. This analysis measures CP violation in $B^- \rightarrow DK^*(892)^-$ decays,¹ with $K^*(892)^- \rightarrow K_s^0(\pi^+\pi^-)\pi^-$, where D denotes a superposition of D^0 and \bar{D}^0 meson states. In this paper K^{*-} is used to represent the $K^*(892)^-$ resonance. The effect of the interference is observed by reconstructing the D meson in a final state accessible to both D^0 and \bar{D}^0 meson states, which gives sensitivity to the weak phase γ . In this analysis, only D mesons decaying to two or four charged kaons and/or pions are considered. The branching fraction of $B^- \rightarrow DK^{*-}$ is of a similar magnitude to $B^- \rightarrow DK^-$, which has been extensively analysed at LHCb [6–8]. However, the reconstruction efficiencies associated with the $K^{*-} \rightarrow K_s^0\pi^-$ decay are lower due to the presence of a long-lived neutral particle.

Two main classes of D decays are used. The first employs D decays into the CP -even eigenstates K^+K^- and $\pi^+\pi^-$; these are referred to here as the ‘‘GLW’’ decay modes [9, 10]. The second class of decay modes involves D decays to $K^\mp\pi^\pm$, which is not a CP eigenstate. In the favoured decay, the pion from the D meson and that from the K^{*-} meson have opposite charge, while in the suppressed decay (referred to here as the ‘‘ADS’’ [11, 12] decay mode) the pion from the D meson that from the K^{*-} meson have the same charge. The favoured mode is used as a control mode for many aspects of the analysis since no CP asymmetry is expected. The ADS decay mode is a combination of a CKM-favoured $B^- \rightarrow D^0K^{*-}$ decay, followed by a doubly Cabibbo-suppressed $D^0 \rightarrow K^+\pi^-$ decay, and a CKM- and colour-suppressed $B^- \rightarrow \bar{D}^0K^{*-}$ decay, followed by a Cabibbo-favoured $\bar{D}^0 \rightarrow K^+\pi^-$ decay. Both paths to the same final state have amplitudes of similar size, and interference effects are therefore magnified in comparison to the GLW decay modes, where the decay path via the CKM-favoured $B^- \rightarrow D^0K^{*-}$ dominates. Studies of $B^- \rightarrow DK^-$ and $B^0 \rightarrow DK^{*0}$ decays have been published by the LHCb collaboration [6, 13].

¹The inclusion of charge-conjugate processes is implied, except when discussing ratios or asymmetries between B^+ and B^- decays.

The GLW and ADS methods can be extended to the $D \rightarrow K^\mp \pi^\pm \pi^\mp \pi^\pm$ and $D \rightarrow \pi^+ \pi^- \pi^+ \pi^-$ inclusive four-body final states, provided external information is available on the overall behaviour of the intermediate resonances, averaged over phase space [14, 15]. These channels have previously been studied for $B^- \rightarrow DK^-$ decays [6], and are included in this paper for the first time in $B^- \rightarrow DK^{*-}$ decays. The $B^- \rightarrow DK^{*-}$ channel has previously been investigated by the BaBar collaboration using a variety of two-body D decay modes [16]. Also, both the BaBar and Belle collaborations have performed studies on $B^- \rightarrow DK^{*-}$ with $D \rightarrow K_s^0 \pi^+ \pi^-$ [17, 18].

Twelve quantities, collectively referred to as CP observables, are measured in this analysis

- The CP asymmetry for the favoured decay mode

$$A_{K\pi} = \frac{\Gamma(B^- \rightarrow D(K^-\pi^+)K^{*-}) - \Gamma(B^+ \rightarrow D(K^+\pi^-)K^{*+})}{\Gamma(B^- \rightarrow D(K^-\pi^+)K^{*-}) + \Gamma(B^+ \rightarrow D(K^+\pi^-)K^{*+})}. \quad (1)$$

- The CP asymmetry for the $D \rightarrow K^+K^-$ decay mode

$$A_{KK} = \frac{\Gamma(B^- \rightarrow D(K^+K^-)K^{*-}) - \Gamma(B^+ \rightarrow D(K^+K^-)K^{*+})}{\Gamma(B^- \rightarrow D(K^+K^-)K^{*-}) + \Gamma(B^+ \rightarrow D(K^+K^-)K^{*+})}. \quad (2)$$

- The CP asymmetry for the $D \rightarrow \pi^+\pi^-$ decay mode

$$A_{\pi\pi} = \frac{\Gamma(B^- \rightarrow D(\pi^+\pi^-)K^{*-}) - \Gamma(B^+ \rightarrow D(\pi^+\pi^-)K^{*+})}{\Gamma(B^- \rightarrow D(\pi^+\pi^-)K^{*-}) + \Gamma(B^+ \rightarrow D(\pi^+\pi^-)K^{*+})}. \quad (3)$$

- The ratio of the rate for the $D \rightarrow K^+K^-$ decay mode to that of the favoured decay mode, scaled by the branching fractions

$$R_{KK} = \frac{\Gamma(B^- \rightarrow D(K^+K^-)K^{*-}) + \Gamma(B^+ \rightarrow D(K^+K^-)K^{*+})}{\Gamma(B^- \rightarrow D(K^-\pi^+)K^{*-}) + \Gamma(B^+ \rightarrow D(K^+\pi^-)K^{*+})} \times \frac{\mathcal{B}(D^0 \rightarrow K^-\pi^+)}{\mathcal{B}(D^0 \rightarrow K^+K^-)}. \quad (4)$$

- The ratio of the rate for the $D \rightarrow \pi^+\pi^-$ decay mode to that of the favoured decay mode, scaled by the branching fractions

$$R_{\pi\pi} = \frac{\Gamma(B^- \rightarrow D(\pi^+\pi^-)K^{*-}) + \Gamma(B^+ \rightarrow D(\pi^+\pi^-)K^{*+})}{\Gamma(B^- \rightarrow D(K^-\pi^+)K^{*-}) + \Gamma(B^+ \rightarrow D(K^+\pi^-)K^{*+})} \times \frac{\mathcal{B}(D^0 \rightarrow K^-\pi^+)}{\mathcal{B}(D^0 \rightarrow \pi^+\pi^-)}. \quad (5)$$

- The ratio of the rate for the ADS decay mode to that of the favoured decay mode for B^+ decays

$$R_{K\pi}^+ = \frac{\Gamma(B^+ \rightarrow D(K^-\pi^+)K^{*+})}{\Gamma(B^+ \rightarrow D(K^+\pi^-)K^{*+})}. \quad (6)$$

- The ratio of the rate for the ADS decay mode to that of the favoured decay mode for B^- decays

$$R_{K\pi}^- = \frac{\Gamma(B^- \rightarrow D(K^+\pi^-)K^{*-})}{\Gamma(B^- \rightarrow D(K^-\pi^+)K^{*-})}. \quad (7)$$

- The CP asymmetry for the favoured $D^0 \rightarrow K^-\pi^+\pi^-\pi^+$ decay mode

$$A_{K\pi\pi\pi} = \frac{\Gamma(B^- \rightarrow D(K^-\pi^+\pi^-\pi^+)K^{*-}) - \Gamma(B^+ \rightarrow D(K^+\pi^-\pi^+\pi^-)K^{*+})}{\Gamma(B^- \rightarrow D(K^-\pi^+\pi^-\pi^+)K^{*-}) + \Gamma(B^+ \rightarrow D(K^+\pi^-\pi^+\pi^-)K^{*+})}. \quad (8)$$

- The CP asymmetry for the $D \rightarrow \pi^+\pi^-\pi^+\pi^-$ decay mode

$$A_{\pi\pi\pi\pi} = \frac{\Gamma(B^- \rightarrow D(\pi^+\pi^-\pi^+\pi^-)K^{*-}) - \Gamma(B^+ \rightarrow D(\pi^+\pi^-\pi^+\pi^-)K^{*+})}{\Gamma(B^- \rightarrow D(\pi^+\pi^-\pi^+\pi^-)K^{*-}) + \Gamma(B^+ \rightarrow D(\pi^+\pi^-\pi^+\pi^-)K^{*+})}. \quad (9)$$

- The ratio of the rate for the $D \rightarrow \pi^+\pi^-\pi^+\pi^-$ decay mode to that of the favoured decay mode, scaled by the branching fractions

$$R_{\pi\pi\pi\pi} = \frac{\Gamma(B^- \rightarrow D(\pi^+\pi^-\pi^+\pi^-)K^{*-}) + \Gamma(B^+ \rightarrow D(\pi^+\pi^-\pi^+\pi^-)K^{*+})}{\Gamma(B^- \rightarrow D(K^-\pi^+\pi^-\pi^+)K^{*-}) + \Gamma(B^+ \rightarrow D(K^+\pi^-\pi^+\pi^-)K^{*+})} \times \frac{\mathcal{B}(D^0 \rightarrow K^-\pi^+\pi^-\pi^+)}{\mathcal{B}(D^0 \rightarrow \pi^+\pi^-\pi^+\pi^-)}. \quad (10)$$

- The ratio of the rate for the four-body ADS decay mode to that of the four-body favoured decay mode for B^+ decays

$$R_{K\pi\pi\pi}^+ = \frac{\Gamma(B^+ \rightarrow D(K^-\pi^+\pi^-\pi^+)K^{*+})}{\Gamma(B^+ \rightarrow D(K^+\pi^-\pi^+\pi^-)K^{*+})}. \quad (11)$$

- The ratio of the rate of the four-body ADS decay mode to that of the four-body favoured decay mode for B^- decays

$$R_{K\pi\pi\pi}^- = \frac{\Gamma(B^- \rightarrow D(K^+\pi^-\pi^+\pi^-)K^{*-})}{\Gamma(B^- \rightarrow D(K^-\pi^+\pi^-\pi^+)K^{*-})}. \quad (12)$$

The asymmetries $A_{K\pi}$ and $A_{K\pi\pi\pi}$ should be essentially zero due to the very small interference expected in the configuration of B and D decays. Due to negligible direct CP violation in D decays [19], the observables A_{KK} and $A_{\pi\pi}$ should be equal and are often labelled together as A_{CP+} ; similarly the observables R_{KK} and $R_{\pi\pi}$ should be equal and are labelled R_{CP+} . The analogous observables to R_{CP+} and A_{CP+} for the ADS mode are R_{ADS} and A_{ADS} . However, R_{ADS} and A_{ADS} are not used for the ADS decay mode, instead the ratios are measured separately for the positive and negative charges. The reason for this choice is that the uncertainty in A_{ADS} depends on the value of R_{ADS} , therefore these observables are statistically dependent, raising problems for the low yields expected in the ADS mode. Hence the statistically independent observables $R_{K\pi}^+$ and $R_{K\pi}^-$ are preferred.

The CP observables measured in this analysis can be related to the physics parameters to be determined, namely γ , r_B and δ_B . The parameter r_B is the ratio of the magnitudes between the suppressed and favoured amplitudes of the B decay and δ_B is the strong-phase difference between these amplitudes. The expected value is $r_B \sim 0.1$, similar to that in the $B^- \rightarrow DK^-$ decay. Both r_B and δ_B are averaged over the region of $DK_s^0\pi^-$ phase space corresponding to the K^{*-} selection window. A coherence factor, κ , accounts for the contribution of $B^- \rightarrow DK_s^0\pi^-$ decays that are not due to an intermediate $K^*(892)^-$ resonance [20], where $\kappa = 1$ denotes a pure $K^*(892)^-$ contribution. Given there is a negligible effect from both charm mixing [21] and CP violation in D decays [19], the relationships between the CP observables and physics parameters are given in the following equations,

$$A_{CP+} = \frac{2\kappa r_B \sin \delta_B \sin \gamma}{1 + r_B^2 + 2\kappa r_B \cos \delta_B \cos \gamma}, \quad (13)$$

$$R_{CP+} = 1 + r_B^2 + 2\kappa r_B \cos \delta_B \cos \gamma , \quad (14)$$

$$R_{K\pi}^{\pm} = \frac{r_B^2 + (r_D^{K\pi})^2 + 2\kappa r_B r_D^{K\pi} \cos(\delta_B + \delta_D^{K\pi} \pm \gamma)}{1 + r_B^2 (r_D^{K\pi})^2 + 2\kappa r_B r_D^{K\pi} \cos(\delta_B - \delta_D^{K\pi} \pm \gamma)} , \quad (15)$$

$$A_{\pi\pi\pi\pi} = \frac{2\kappa (2F_{4\pi} - 1) r_B \sin \delta_B \sin \gamma}{1 + r_B^2 + 2\kappa (2F_{4\pi} - 1) r_B \cos \delta_B \cos \gamma} , \quad (16)$$

$$R_{\pi\pi\pi\pi} = 1 + r_B^2 + 2\kappa (2F_{4\pi} - 1) r_B \cos \delta_B \cos \gamma , \quad (17)$$

$$R_{K\pi\pi\pi}^{\pm} = \frac{r_B^2 + (r_D^{K3\pi})^2 + 2\kappa r_B \kappa_{K3\pi} r_D^{K3\pi} \cos(\delta_B + \delta_D^{K3\pi} \pm \gamma)}{1 + (r_B r_D^{K3\pi})^2 + 2\kappa r_B \kappa_{K3\pi} r_D^{K3\pi} \cos(\delta_B - \delta_D^{K3\pi} \pm \gamma)} . \quad (18)$$

These relationships depend on several parameters describing the D decays, which are taken from existing measurements. The parameters $r_D^{K\pi}$ and $\delta_D^{K\pi}$ are the magnitude of the amplitude ratio and the strong-phase difference between the suppressed and favoured amplitudes of the D decay, namely $D^0 \rightarrow K^+\pi^-$ and $D^0 \rightarrow K^-\pi^+$ respectively [22]. Similarly, the parameters $r_D^{K3\pi}$ and $\delta_D^{K3\pi}$ are the equivalent quantities for the decays $D^0 \rightarrow K^+\pi^-\pi^+\pi^-$ and $D^0 \rightarrow K^-\pi^+\pi^-\pi^+$, averaged over phase space [23, 24]. Two-body $D \rightarrow K^\mp\pi^\pm$ decays are characterised by a single strong phase, however for multibody $D \rightarrow K^\mp\pi^\pm\pi^\mp\pi^\pm$ decays the strong phase varies over the phase space. By averaging the strong phase variation the interference effects are diluted. This effect is accounted for by the parameter $\kappa_{K3\pi}$ [23, 24]. The parameter $F_{4\pi} \sim 0.75$ [15] accounts for the fact that $D \rightarrow \pi^+\pi^-\pi^+\pi^-$, though predominantly CP even, is not a pure CP eigenstate.

2 Detector, online selection and simulation

The LHCb detector [25, 26] is a single-arm forward spectrometer covering the pseudorapidity range $2 < \eta < 5$, designed for the study of particles containing b or c quarks. The detector includes a high-precision tracking system consisting of a silicon-strip vertex detector (VELO) surrounding the pp interaction region, a large-area silicon-strip detector (TT) located upstream of a dipole magnet with a bending power of about 4 Tm, and three stations of silicon-strip detectors and straw drift tubes placed downstream of the magnet. The tracking system provides a measurement of momentum, p , of charged particles with a relative uncertainty that varies from 0.5% at low momentum to 1.0% at 200 GeV/ c . The minimum distance of a track to a primary vertex (PV), the impact parameter (IP), is measured with a resolution of $(15 + 29/p_T) \mu\text{m}$, where p_T is the component of the momentum transverse to the beam, in GeV/ c . Different types of charged hadrons are distinguished using information from two ring-imaging Cherenkov detectors (RICH). Photons, electrons and hadrons are identified by a calorimeter system consisting of scintillating-pad and preshower detectors, an electromagnetic calorimeter and a hadronic calorimeter. Muons are identified by a system composed of alternating layers of iron and multiwire proportional chambers, and gas electron multiplier detectors.

The online event selection is performed by a trigger [27], which consists of a hardware stage, based on information from the calorimeter and muon systems, followed by a software

stage, which applies a full event reconstruction. Signal events considered in the analysis must fulfil hardware and software trigger requirements. At the hardware trigger stage, events are required to have a muon with high p_T or a hadron, photon or electron with high transverse energy in the calorimeters. At the software stage, at least one charged particle should have high p_T and large χ_{IP}^2 with respect to any PV, where χ_{IP}^2 is defined as the difference in the vertex-fit χ^2 of a given PV fitted with and without the considered track. The software trigger designed to select b -hadron decays uses a multivariate algorithm [28] to identify a two-, three- or four-track secondary vertex with a large scalar sum of the p_T of the associated charged particles and a significant displacement from the PVs. The PVs are fitted with and without the B candidate, and the PV with the smallest χ_{IP}^2 is associated with the B candidate.

The analysis presented is based on pp collision data corresponding to an integrated luminosity of 1 fb^{-1} at a centre-of-mass energy of 7 TeV collected in 2011, 2 fb^{-1} at 8 TeV collected in 2012 (jointly referred to as Run 1), and 1.8 fb^{-1} at 13 TeV collected in 2015 and 2016 (referred to as Run 2). There are several differences between data collected in Run 1 and Run 2. The main difference is the higher $b\bar{b}$ production cross-section in Run 2 [29]. The average number of pp interactions per bunch crossing is reduced to 1.1 in Run 2 compared to 1.7 in Run 1. The net effect is that, despite the higher energy of the collisions, the background levels and signal-to-background ratios in Run 1 and Run 2 for the type of decay analysed here are similar. Before the start of Run 2, the aerogel radiator was removed from the first RICH detector [30], which improves the detector resolution. Hence, for momenta typical of decays in this analysis, the particle identification criteria have resulted in an increased efficiency of signal selection while simultaneously decreasing the rate of misidentified backgrounds. For the $B^- \rightarrow D(K^-\pi^+)K^{*-}$ decay mode, the combination of higher $b\bar{b}$ production cross-section, improved particle identification and improvements to the online selection in Run 2 have resulted in a factor of three increase in the yield for a given integrated luminosity.

Simulated event samples are used for the study of efficiencies. In the simulation, pp collisions are generated using PYTHIA [31] with a specific LHCb configuration [32]. Decays of hadronic particles are described by EVTGEN [33], in which final-state radiation is generated using PHOTOS [34]. The interaction of the generated particles with the detector, and its response, are implemented using the GEANT4 toolkit [35] as described in Ref. [36].

3 Offline selection

The K^{*-} meson is reconstructed in the decay $K^{*-} \rightarrow K_s^0\pi^-$ and the K_s^0 meson is reconstructed through its decay to two charged pions. If the pions from the K_s^0 decay leave sufficient hits in the VELO to be included in the track reconstruction, the reconstructed K_s^0 meson is called “long”. Due to the high boost from the pp collision many K_s^0 particles decay outside the VELO. If the pions from the K_s^0 decay do not leave sufficient hits in the VELO, the reconstructed K_s^0 meson is called “downstream”, with the first hits being recorded in the TT, which typically results in poorer mass resolution. These K_s^0 reconstruction types are treated as separate data samples and a slightly different selection is applied to each.

Reconstructed B candidates are formed by combining a K^{*-} candidate with a D

candidate, which are required to form a good-quality vertex. For each D , K^{*-} , and K_s^0 candidate the reconstructed meson masses are required to lie within $25 \text{ MeV}/c^2$ around the D mass, $75 \text{ MeV}/c^2$ around the K^{*-} mass, and $15 \text{ MeV}/c^2$ around the K_s^0 mass for long candidates and $20 \text{ MeV}/c^2$ for downstream candidates [37]. A kinematic fit [38] is performed on the full B decay chain constraining the B candidate to point towards the PV, and the D and K_s^0 candidates to have their known masses [37]. To suppress charmless backgrounds, the D decay vertex is required to be well-separated from and downstream of the B^- decay vertex. Also, the K_s^0 decay vertex is required to be well-separated from and downstream of the B^- decay vertex in order to suppress $B^- \rightarrow D\pi^-\pi^+\pi^-$ decays. The selection window of $\pm 75 \text{ MeV}/c^2$, 1.5 times the $K^*(892)^-$ natural width, is required to suppress $B^- \rightarrow DK_s^0\pi^-$ decays that do not proceed via an intermediate $K^*(892)^-$ resonance. Further suppression of these decays is achieved by requiring the magnitude of the cosine of the K_s^0 helicity angle to be greater than 0.3. The K_s^0 helicity angle is defined as the angle between the K_s^0 and the B^- momentum vectors in the K^{*-} rest frame. This requirement retains 97% of true K^{*-} decays, which are distributed parabolically in this variable, while rejecting 30% of the background.

Requirements, based mainly on the RICH system, are applied to all D decay products to identify them as kaons or pions. These selections are applied such that each D candidate is assigned a unique category. Cross-feed between the $K^-\pi^+$, K^+K^- and $\pi^+\pi^-$ D final states is negligible because after misidentification of a π^- meson as a K^- meson (or vice versa) the reconstructed mass of the D meson lies outside the D mass selection window. However, the favoured decay $B^- \rightarrow D(K^-\pi^+)K^{*-}$ can appear in the $B^- \rightarrow D(\pi^-K^+)K^{*-}$ sample due to misidentification of both D decay products. To suppress this, a veto is applied to the ADS decay mode. The D mass is reconstructed assuming the mass hypotheses of the decay products are swapped. If the resulting value is within $15 \text{ MeV}/c^2$ of the nominal D mass, the candidate is removed from the sample, after which any remaining contamination is negligible while retaining 92% of the signal. Similarly a $15 \text{ MeV}/c^2$ veto selection is applied to the four-body ADS decay mode to prevent the contamination of $B^- \rightarrow D(K^-\pi^+\pi^-\pi^+)K^{*-}$ in the $B^- \rightarrow D(\pi^-K^+\pi^-\pi^+)K^{*-}$ sample. The swapped D mass hypothesis is considered for both π^+ mesons separately, resulting in a combined signal efficiency for the vetoes of 90%.

Combinatorial background is suppressed using a Boosted Decision Tree (BDT) multivariate discriminant [39]. To train the BDT for two-body decays, simulated $B^- \rightarrow D(K^-\pi^+)K^{*-}$ candidates are used as a signal sample and events from the high-mass sideband region of the B^- mass, above $5600 \text{ MeV}/c^2$, in the favoured $B^- \rightarrow D(K^-\pi^+)K^{*-}$ decay mode are used as a sample of combinatorial background. An analogous strategy is employed in the BDT for four-body decays. Various input quantities are used to exploit the topology of the decay; of particular importance are the B^- vertex-fit χ^2 and the p_T asymmetry between the B^- candidate and other tracks from the same PV, defined as

$$Ap_T = \frac{p_T^B - p_T^{\text{cone}}}{p_T^B + p_T^{\text{cone}}} \quad (19)$$

where p_T^B is the p_T of the reconstructed B^- signal candidate and p_T^{cone} is the scalar sum of the p_T of all other tracks in a cone surrounding the B^- candidate. This asymmetry is a quantitative measure of the isolation of the B^- candidate. Other input quantities used include the logarithm of the χ_{IP}^2 for various particles and the p_T of the K_s^0 candidate (for downstream candidates only). The selection requirement on the BDT output was

chosen to minimise the uncertainty on the CP observables. The optimisation is performed separately for the GLW and ADS decay modes. Averaged across the whole dataset used for the analysis, the BDT selection applied to the favoured $B^- \rightarrow D(K^-\pi^+)K^{*-}$ channel gives a signal efficiency of 95% (90%) and a background rejection of 94% (95%) for long (downstream) candidates. Similarly, the four-body favoured $B^- \rightarrow D(K^-\pi^+\pi^-\pi^+)K^{*-}$ channel gives a signal efficiency of 95% (93%) and a background rejection of 96% (97%) for long (downstream) candidates.

4 Fit to the invariant mass distribution

Extended unbinned maximum likelihood fits are applied to the B candidate mass spectra, in the mass range 4900–5600 MeV/ c^2 , for candidates reconstructed in the favoured decay modes $B^- \rightarrow D(K^-\pi^+)K^{*-}$ and $B^- \rightarrow D(K^-\pi^+\pi^-\pi^+)K^{*-}$. The same fit model is applied to both spectra. The model consists of a signal component, backgrounds from partially reconstructed decays and a combinatorial background shape. The charmless background has been suppressed to negligible levels, therefore no component is included in the fit. The signal component is described by the sum of two Crystal Ball (CB) functions [40] with the same peak position, which contain small radiative tails that extend towards lower invariant mass. The signal shape parameters are determined from simulation, except for the common peak position and one of the widths, which are allowed to vary in the fit. The combinatorial background is described by an exponential function. The results of these fits are shown in Fig. 1.

Backgrounds from partially reconstructed decays include $B \rightarrow D^*K^*$ decays where a pion or photon is not reconstructed, namely $B^- \rightarrow D^{*0}(D^0\pi^0)K^{*-}$, $B^- \rightarrow D^{*0}(D^0\gamma)K^{*-}$ and $\bar{B}^0 \rightarrow D^{*+}(D^0\pi^+)K^{*-}$. These are decays of B mesons into two vector particles, which are described by three independent helicity amplitudes, corresponding to the helicity states of the D^* meson, denoted by -1 , 0 and $+1$. The reconstructed B -candidate mass distributions for -1 and $+1$ helicity states are indistinguishable so these states are collectively named ± 1 . Therefore, for each D^*K^{*-} channel, two different components are considered, 0 and ± 1 . The shape of these components are determined from simulations and parameterised as Gaussian functions convolved with a second-order polynomial, described in detail in Ref. [41, 42], with all parameters fixed in the fit. The ratio between the yields of the three D^*K^{*-} decay modes are fixed according to their branching fractions and selection efficiencies, assuming no CP violation. This procedure assumes that the longitudinal polarisation fraction for D^*K^{*-} decays is the same for \bar{B}^0 and B^- mesons. The total partially reconstructed yield is allowed to vary as well as the yield ratio between the sum of the 0 shapes and the sum of the ± 1 shapes.

As seen from the fit projections in Fig. 1, these background contributions are sufficient to describe the overall invariant mass distribution of the favoured decay mode. A number of other backgrounds which could appear close to the signal peak are studied in simulation and found to be negligible, for example $B^- \rightarrow DK^{*-}\pi^0$ and $B^- \rightarrow D(K_S^0\pi\pi)K^-$. Figure 1 shows that the main background contribution near the signal peak is combinatorial background, while only a small amount of partially reconstructed background enters the signal region. A significant fraction of the combinatorial background is expected to come from $B^- \rightarrow D\pi^-X$ decays combined with a real but unrelated K_S^0 meson, which is consistent with the observed difference in background level between the $B^- \rightarrow D(K^-\pi^+)K^{*-}$ and

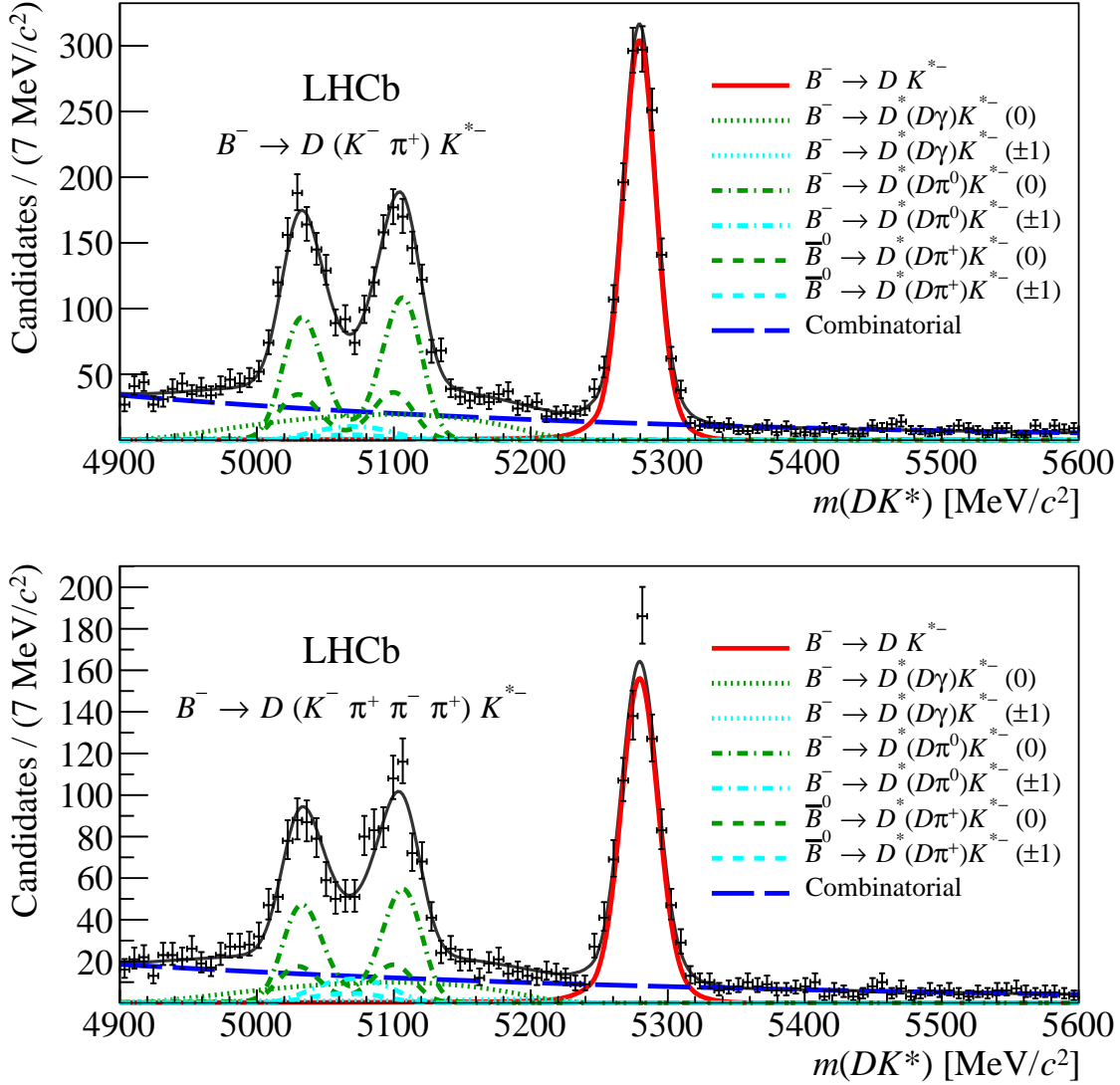


Figure 1: Invariant mass distribution with the fit result superimposed for the favoured $B^- \rightarrow D(K^- \pi^+) K^{*-}$ decay mode (top), and $B^- \rightarrow D(K^- \pi^+ \pi^- \pi^+) K^{*-}$ decay mode (bottom), using Run 1 and Run 2 data combined. The labels 0 and ± 1 correspond to the helicity state of the D^* meson.

$B^- \rightarrow D(K^+ \pi^-) K^{*-}$ decay modes. In the case of the $B^- \rightarrow D(K^+ K^-) K^{*-}$ decay mode, an additional background coming from the decay $\Lambda_b^0 \rightarrow \Lambda_c^+(p K^- \pi^+) K^{*-}$ needs to be considered, where the π^+ meson is not reconstructed and the proton is misidentified as a kaon. The shape of this background is obtained by parameterising the mass distribution from simulated background events; the shape parameters are fixed in the fits described below. The yield of $\Lambda_b^0 \rightarrow \Lambda_c^+(p K^- \pi^+) K^{*-}$ compared to signal in the $B^- \rightarrow D(K^- \pi^+) K^{*-}$ favoured decay mode is allowed to vary.

Restricting the lower limit of the mass range to $5230 \text{ MeV}/c^2$ removes 0.4% of signal and avoids the need to fit the backgrounds from partially reconstructed decays in each of the decay modes. This strategy improves fit stability in the decay modes with lower yields. The shape and yield of the small amount of background from partially reconstructed

decays present in all D decay categories above $5230 \text{ MeV}/c^2$ is determined and fixed from the fit to data with the favoured decay, adjusted for the smaller branching fractions of the rarer D decays. The yield is estimated to be less than one candidate for all CP -violating decay modes, and therefore uncertainties due to the assumptions present in the initial fit have a very small effect. These uncertainties in the yield, shape and possible asymmetries in the distribution between B^+ and B^- are sources of systematic uncertainty.

A simultaneous fit is performed to 56 B -meson mass distributions, corresponding to each of the seven D decay modes ($K^-\pi^+$, K^+K^- , $\pi^+\pi^-$, $K^+\pi^-$, $K^-\pi^+\pi^-\pi^+$, $\pi^+\pi^-\pi^+\pi^-$ and $K^+\pi^-\pi^+\pi^-$), two B -meson charges (B^+ and B^-), two K_S^0 reconstruction types (long and downstream) and two periods of data taking (Run 1 and Run 2). Based on fits to the data and simulation samples, the same signal peak position and width are used for the two periods of data taking, B -meson charges and K_S^0 reconstruction types, but they are allowed to differ between two- and four-body decay modes. The combinatorial background slope is required to have the same value for all two- and four-body decay modes separately, but can differ between long and downstream categories.

The parameters determined from the simultaneous fit are the yields in the favoured signal decay modes and the CP observables $A_{K\pi}$, A_{KK} , $A_{\pi\pi}$, R_{KK} , $R_{\pi\pi}$, $R_{K\pi}^+$, $R_{K\pi}^-$, $A_{K\pi\pi\pi}$, $A_{\pi\pi\pi\pi}$, $R_{\pi\pi\pi\pi}$, $R_{K\pi\pi\pi}^+$ and $R_{K\pi\pi\pi}^-$. The observables are related to the ratios between the yields through various efficiency corrections, given by

$$R_{hh} = \frac{N(B^- \rightarrow D(h^+h^-)K^{*-})}{N(B^- \rightarrow D(K^-\pi^+)K^{*-})} \times \frac{\mathcal{B}(D^0 \rightarrow K^-\pi^+)}{\mathcal{B}(D^0 \rightarrow hh)} \times \frac{\epsilon_{\text{sel}}(K\pi)}{\epsilon_{\text{sel}}(hh)} \times \frac{\epsilon_{\text{PID}}(K\pi)}{\epsilon_{\text{PID}}(hh)}, \quad (20)$$

$$R_{K\pi}^\pm = \frac{N(B^\pm \rightarrow D(K^\mp\pi^\pm)K^{*\pm})}{N(B^\pm \rightarrow D(K^\pm\pi^\mp)K^{*\pm})} \times \frac{\epsilon_{\text{sel}}(K\pi)}{\epsilon_{\text{sel}}(\pi K)} \times \frac{1}{\epsilon_{\text{veto}}(\pi K)}, \quad (21)$$

$$R_{\pi\pi\pi\pi} = \frac{N(B^- \rightarrow D(\pi^+\pi^-\pi^+\pi^-)K^{*-})}{N(B^- \rightarrow D(K^-\pi^+\pi^-\pi^+)K^{*-})} \times \frac{\mathcal{B}(D^0 \rightarrow K^-\pi^+\pi^-\pi^+)}{\mathcal{B}(D^0 \rightarrow \pi\pi\pi\pi)} \times \frac{\epsilon_{\text{sel}}(K\pi\pi\pi)}{\epsilon_{\text{sel}}(\pi\pi\pi\pi)} \times \frac{\epsilon_{\text{PID}}(K\pi\pi\pi)}{\epsilon_{\text{PID}}(\pi\pi\pi\pi)}, \quad (22)$$

$$R_{K\pi\pi\pi}^\pm = \frac{N(B^\pm \rightarrow D(K^\mp\pi^\pm\pi^\mp\pi^\pm)K^{*\pm})}{N(B^\pm \rightarrow D(K^\pm\pi^\mp\pi^\pm\pi^\mp)K^{*\pm})} \times \frac{\epsilon_{\text{sel}}(K\pi\pi\pi)}{\epsilon_{\text{sel}}(\pi K\pi\pi)} \times \frac{1}{\epsilon_{\text{veto}}(\pi K\pi\pi)}, \quad (23)$$

where ϵ_{sel} , ϵ_{PID} and ϵ_{veto} are the selection, particle-identification and veto efficiencies, respectively, N is the yield of the specified decay and h represents a π or K meson. The veto is only applied to the ADS decay mode to reduce cross-feed from the favoured decay. These efficiencies are determined from simulation. The selection efficiency for various D decay modes accounts for any differences in kinematics between these modes as well as a tighter BDT cut in the ADS decay mode, which is applied in order to optimise the uncertainty in the CP observables. Any further correction to the four-body observables due to nonuniform acceptance was found to be negligible. The efficiencies cancel for the determination of the CP asymmetries, while corrections are applied for the B^+ , B^- production asymmetry, A_{prod} , and decay mode dependent detection asymmetries, A_{det} , which are taken from previous LHCb measurements for production asymmetry [43], kaon detection asymmetry [44] and pion detection asymmetry [45]. The value A_{prod} is assumed to be the same for 7 TeV, 8 TeV and 13 TeV data. A possible difference in A_{prod} for Run 2 data compared to Run 1 is accounted for as a systematic uncertainty. As the asymmetries are small, $\mathcal{O}(1\%)$ or less, the observed uncorrected asymmetry A_{raw} can be expressed as the sum $A_{\text{raw}} = A_{\text{phys}} + A_{\text{prod}} + A_{\text{det}}$, where A_{phys} is the CP asymmetry to be extracted. Hence, A_{prod} and A_{det} provide additive corrections to the measured asymmetry.

Table 1: Fitted yields in each of the B decay modes. The uncertainties are statistical only.

Decay mode	B^- yield	B^+ yield
$B^\pm \rightarrow D(K^\pm \pi^\mp) K^{*\pm}$	996 ± 34	1035 ± 35
$B^\pm \rightarrow D(K^+ K^-) K^{*\pm}$	134 ± 14	121 ± 13
$B^\pm \rightarrow D(\pi^+ \pi^-) K^{*\pm}$	45 ± 10	33 ± 9
$B^\pm \rightarrow D(K^\mp \pi^\pm) K^{*\pm}$	1.6 ± 1.9	19 ± 7
$B^\pm \rightarrow D(K^\pm \pi^\mp \pi^+ \pi^-) K^{*\pm}$	556 ± 26	588 ± 27
$B^\pm \rightarrow D(\pi^+ \pi^- \pi^+ \pi^-) K^{*\pm}$	59 ± 10	56 ± 10
$B^\pm \rightarrow D(K^\mp \pi^\pm \pi^- \pi^+) K^{*\pm}$	3 ± 5	10 ± 6

5 Results

The invariant mass spectra and resulting fits to data, combining Run 1, Run 2, long and downstream categories, are shown in Figs. 2 and 3. The yields determined from the fitted parameters are given in Table 1. The Wilks' theorem statistical significance [46] for the two-body ADS decay mode is 4.2σ , while for the four-body ADS decay mode it is 2.8σ . This represents the first evidence of the two-body suppressed decay.

Branching fractions [37], various efficiencies and asymmetries are used as inputs to the simultaneous fit in order to relate the measured yields to the CP observables. Each of these inputs has an associated uncertainty which needs to be propagated to the CP observables giving rise to the systematic uncertainties. In the case of the efficiencies, uncertainties arise from a limited sample size of simulated events. Uncertainties on A_{prod} and A_{det} are taken from previous LHCb measurements in Run 1 [43–45]. The changes to the detector between the data-taking periods are not expected to significantly affect the A_{det} measurement. For A_{prod} , a conservative estimate, double the Run 1 uncertainty, is assigned to accommodate a possible dependence of the production asymmetry on the centre-of-mass energy. The systematic uncertainties due to the use of fixed inputs from branching ratios, simulation efficiencies, asymmetry corrections and shape parameters are estimated by performing multiple fits to data where each relevant parameter is varied according to a Gaussian distribution with the width as the assigned uncertainty. The standard deviation of the fitted parameter distribution is assigned as the systematic uncertainty. Correlations between the shape parameters are small, typically less than 10%, and are ignored. Tests, where the most relevant correlations have been included, show a negligible impact on the systematic uncertainty arising from the fixed shape parameters.

Other systematic uncertainties arise from the modelling of the signal and partially reconstructed backgrounds and the effect of any residual charmless B decays. The systematic uncertainties from these sources are computed by generating pseudoexperiments. In each case the generated model is varied according to the systematic effects being estimated. The systematic uncertainty on each observable is taken to be the difference between the mean of the fitted parameter distribution and the generated value. The systematic uncertainty on the partially reconstructed background takes into account uncertainties in the yield and shape parameters, as well as possible asymmetries due to CP violation. The contamination from charmless B decays is consistent with zero, although it has a large uncertainty. Pseudoexperiments are generated with charmless decays according

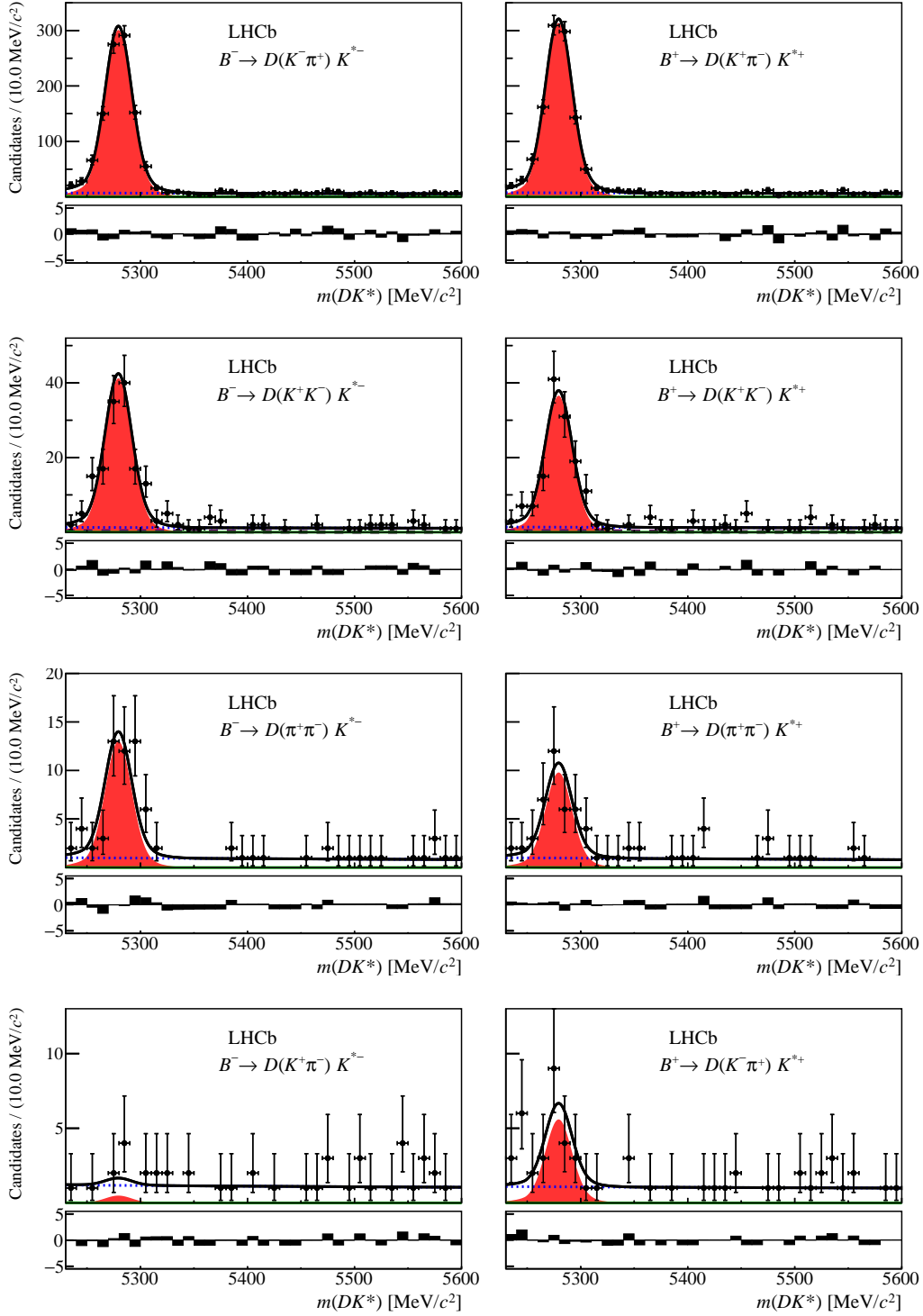


Figure 2: Result of fits to data for the two-body decay modes with Run 1, Run 2, long and downstream categories summed for presentation. The signal is represented by the red shaded area, the combinatorial background by the dotted blue line and the partially reconstructed background by the solid green line. In the $D^0 \rightarrow K^+ K^-$ fits the $\Lambda_b^0 \rightarrow \Lambda_c^+ K^{*-}$ background is represented by the dashed purple line. The total fit is given by the black line. The residuals, shown below each plot, are defined as the difference between the data and the fit value in each bin, normalised by the uncertainty.

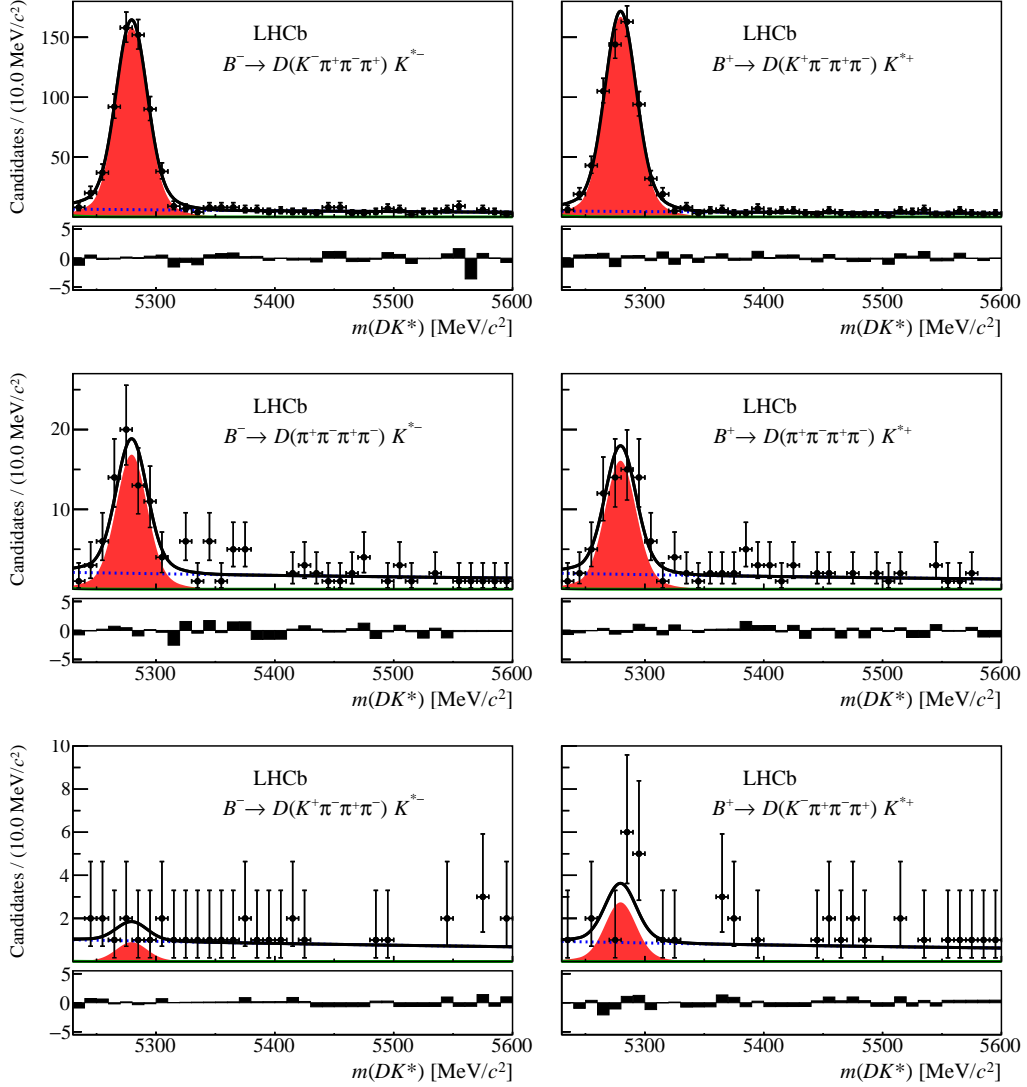


Figure 3: Result of fits to data for the four-body decay modes with Run 1, Run 2, long and downstream categories summed for presentation. The signal is represented by the red shaded area, the combinatorial background by the dotted blue line and the partially reconstructed background by the solid green line. The total fit is given by the black line. The residuals are shown below each plot.

to the fit model, with the number of events fluctuating according to the uncertainty in the fit. The assumption that the slope of the function describing the combinatorial background is the same for all D decay modes has an associated uncertainty. Pseudoexperiments are generated fixing the slope parameters to a different value for each decay mode, where the value used is obtained from fits in the mass region above the B mass. For the ADS mode, a potential background from $B_s^0 \rightarrow D(K^*(1410)^0 \rightarrow K^*(892)^-\pi^+)$, where the π^+ meson is not reconstructed, is considered. An estimate of the contribution using simulated events and the branching fraction [47] is found to be 2.6 ± 2.6 events, which is consistent with observations from data in the region of B mass below the lower limit of the simultaneous fit. The shape of this background is obtained by parameterising the mass distribution from simulated events. A systematic is assigned by performing many fits to data varying the yield according to a Gaussian distribution with the width as the assigned uncertainty. The standard deviation of the fitted parameter distribution is assigned as the systematic uncertainty. A summary of the components of the systematic uncertainties for the CP observables is given in Table 2.

The CP observables determined from the fit shown in Figs. 2 and 3 are

$$\begin{aligned}
A_{K\pi} &= -0.004 \pm 0.023 \pm 0.008 \\
A_{KK} &= 0.06 \pm 0.07 \pm 0.01 \\
A_{\pi\pi} &= 0.15 \pm 0.13 \pm 0.01 \\
R_{KK} &= 1.22 \pm 0.09 \pm 0.02 \\
R_{\pi\pi} &= 1.08 \pm 0.14 \pm 0.03 \\
R_{K\pi}^+ &= 0.020 \pm 0.006 \pm 0.001 \\
R_{K\pi}^- &= 0.002 \pm 0.004 \pm 0.001 \\
A_{K\pi\pi\pi} &= -0.013 \pm 0.031 \pm 0.009 \\
A_{\pi\pi\pi\pi} &= 0.02 \pm 0.11 \pm 0.01 \\
R_{\pi\pi\pi\pi} &= 1.08 \pm 0.13 \pm 0.03 \\
R_{K\pi\pi\pi}^+ &= 0.016 \pm 0.007 \pm 0.003 \\
R_{K\pi\pi\pi}^- &= 0.006 \pm 0.006 \pm 0.004
\end{aligned}$$

where the first uncertainty is statistical and the second is systematic. The correlation matrices for the statistical and systematic uncertainties are given in Tables 3 and 4, respectively. The large correlations of the systematic uncertainties are mainly due to contributions from production and detection asymmetries. Combined results from the K^+K^- and $\pi^+\pi^-$ decay modes, taking correlations into account, are

$$\begin{aligned}
R_{CP+} &= 1.18 \pm 0.08 \pm 0.02 \\
A_{CP+} &= 0.08 \pm 0.06 \pm 0.01
\end{aligned}$$

where the first uncertainty is statistical and the second is systematic. In addition, R^+ and R^- for the $K^+\pi^-$ and $K^+\pi^-\pi^+\pi^-$ decay modes can be transformed into the more commonly used $R_{ADS} = (R^- + R^+)/2$ and $A_{ADS} = (R^- - R^+)/ (R^- + R^+)$. These

Table 2: Summary of systematic uncertainties. Uncertainties are not shown if they are more than two orders of magnitude smaller than the statistical uncertainty.

	$A_{K\pi}$	A_{KK}	$A_{\pi\pi}$	R_{KK}	$R_{\pi\pi}$	$R_{K\pi}^+$	$R_{K\pi}^-$	$A_{K\pi\pi}$	$A_{\pi\pi\pi}$	$R_{\pi\pi\pi}$	$R_{K\pi\pi}^+$	$R_{K\pi\pi}^-$
Statistical	0.023	0.07	0.13	0.09	0.15	0.006	0.004	0.031	0.11	0.13	0.008	0.007
Branching fractions	—	—	0.001	0.013	0.012	—	—	—	0.0008	0.027	—	—
Selection efficiencies	—	—	—	0.007	0.006	0.0002	—	—	0.0008	0.014	—	—
PID efficiencies	—	—	—	0.002	0.002	—	—	—	—	0.002	—	—
Veto efficiencies	—	—	—	—	—	0.0001	—	—	—	—	—	—
A_{prod}	0.0073	0.007	0.008	—	—	—	—	0.0079	0.0077	—	—	—
A_{det}	0.0034	0.003	0.003	—	—	0.0001	—	0.0034	0.0030	—	0.0001	—
Signal shape	0.0011	0.003	0.003	0.011	0.027	0.0011	0.0013	0.0017	0.0022	0.010	0.0030	0.0038
Combinatorial shape	0.0012	0.003	0.005	0.004	0.009	0.0002	0.0003	0.0001	0.0018	—	0.0012	0.0004
Partially reconstructed shape	0.0007	0.001	0.003	0.001	0.005	—	0.0003	0.0003	0.0005	0.002	0.0008	0.0001
Charmless	0.0008	—	0.003	0.002	0.007	—	0.0003	0.0009	0.0030	0.002	0.0008	0.0001
$A_b^0 \rightarrow A_c^+ K^{*-}$	0.0002	—	—	0.011	0.001	0.0001	—	—	—	—	—	—
$B_s^0 \rightarrow DK^*(1410)^0$	—	—	—	—	—	0.0005	0.0001	—	—	—	—	—
Total systematic	0.0083	0.009	0.012	0.022	0.032	0.0012	0.0014	0.0088	0.0093	0.032	0.0034	0.0038

results, taking correlations into account, are

$$\begin{aligned}
R_{ADS}^{K\pi} &= 0.011 \pm 0.004 \pm 0.001 \\
A_{ADS}^{K\pi} &= -0.81 \pm 0.17 \pm 0.04 \\
R_{ADS}^{K\pi\pi\pi} &= 0.011 \pm 0.005 \pm 0.003 \\
A_{ADS}^{K\pi\pi\pi} &= -0.45 \pm 0.21 \pm 0.14
\end{aligned}$$

where the first uncertainty is statistical and the second is systematic. The measured asymmetries and ratios for the two-body D meson decay modes are consistent with, and more precise than, the previous measurements from BaBar [16].

Table 3: Correlation matrix of the statistical uncertainties for the twelve physics observables from the simultaneous fit to data. Only half of the symmetric matrix is shown.

	$A_{K\pi}$	A_{KK}	$A_{\pi\pi}$	R_{KK}	$R_{\pi\pi}$	$R_{K\pi}^+$	$R_{K\pi}^-$	$A_{K\pi\pi\pi}$	$A_{\pi\pi\pi\pi}$	$R_{\pi\pi\pi\pi}$	$R_{K\pi\pi\pi}^+$	$R_{K\pi\pi\pi}^-$
$A_{K\pi}$	1	—	—	—	—	0.08	-0.01	—	—	—	—	—
A_{KK}		1	—	—	—	—	—	—	—	—	—	—
$A_{\pi\pi}$			1	—	-0.02	—	—	—	—	—	—	—
R_{KK}				1	0.05	0.02	-0.01	—	—	—	—	—
$R_{\pi\pi}$					1	0.03	0.02	—	—	—	—	—
$R_{K\pi}^+$						1	0.02	—	—	—	—	—
$R_{K\pi}^-$							1	—	—	—	—	—
$A_{K\pi\pi\pi}$								1	—	—	0.07	-0.03
$A_{\pi\pi\pi\pi}$									1	0.01	—	—
$R_{\pi\pi\pi\pi}$										1	0.04	0.04
$R_{K\pi\pi\pi}^+$											1	0.03
$R_{K\pi\pi\pi}^-$												1

Table 4: Correlation matrix of the systematic uncertainties for the twelve physics observables from the simultaneous fit to data. Only half of the symmetric matrix is shown.

	$A_{K\pi}$	A_{KK}	$A_{\pi\pi}$	R_{KK}	$R_{\pi\pi}$	$R_{K\pi}^+$	$R_{K\pi}^-$	$A_{K\pi\pi\pi}$	$A_{\pi\pi\pi\pi}$	$R_{\pi\pi\pi\pi}$	$R_{K\pi\pi\pi}^+$	$R_{K\pi\pi\pi}^-$
$A_{K\pi}$	1	0.82	0.72	—	—	0.01	-0.02	0.94	0.84	—	-0.01	—
A_{KK}		1	0.65	-0.04	—	0.01	-0.02	0.83	0.77	—	—	—
$A_{\pi\pi}$			1	—	-0.03	—	-0.02	0.72	0.68	—	—	0.01
R_{KK}				1	—	0.05	0.03	-0.01	—	-0.01	-0.01	-0.01
$R_{\pi\pi}$					1	0.06	0.08	-0.01	—	-0.01	-0.02	0.01
$R_{K\pi}^+$						1	0.08	-0.01	—	—	-0.01	-0.01
$R_{K\pi}^-$							1	-0.01	-0.01	-0.01	0.01	0.03
$A_{K\pi\pi\pi}$								1	0.84	—	-0.01	-0.02
$A_{\pi\pi\pi\pi}$									1	0.03	0.01	—
$R_{\pi\pi\pi\pi}$										1	0.01	-0.01
$R_{K\pi\pi\pi}^+$											1	0.05
$R_{K\pi\pi\pi}^-$												1

6 Interpretation

The CP observables measured in this analysis can be used to determine the physics parameters r_B , δ_B and γ , via Eqs. 13-18. The parameter κ is estimated by generating many amplitude models for $B \rightarrow DK_S^0 \pi$ decays [48] consisting of various resonant components whose relative amplitudes and phases are varied within limits according to the existing branching fraction measurements. The components used in the model are $B^- \rightarrow D^0 K^*(892)^-$ and the LASS lineshape [49]. The LASS lineshape is used to describe the $K\pi$ S-wave, which includes a nonresonant term and the $K_0^*(1430)^-$ resonance. Contributions from other resonances *e.g.* $K^*(1680)^- \rightarrow K_S^0 \pi^-$ and $D_2^*(2460)^- \rightarrow D\pi^-$, are considered to be negligible in the selected K^{*-} region and are not included in the model. For each model, the value of κ is determined in the region of phase space defined by the K^{*-} mass window and K_S^0 helicity angle requirements. The mean of the resulting distribution gives an estimate for κ of 0.95 ± 0.06 . The parameters $r_D^{K\pi}$, $\delta_D^{K\pi}$, $r_D^{K3\pi}$, $\delta_D^{K3\pi}$, $\kappa_{K3\pi}$ and $F_{4\pi}$ are also required as external inputs and are taken from Ref. [15, 22–24].

Using the measured values of the CP observables, their uncertainties and the covariance matrices, a global χ^2 minimisation is performed, resulting in a minimum χ^2 of 3.0 with 9 degrees of freedom. A scan of physics parameters is performed for a range of values and the difference in χ^2 between the parameter scan values and the global minimum, $\Delta\chi^2$, is evaluated. The confidence level for any pair of parameters is calculated assuming that these are normally distributed, which enables the $\Delta\chi^2 = 2.30, 6.18, 11.8$ contours to be drawn, corresponding to 68.3%, 95.5%, 99.7% confidence levels, respectively. These are shown in Fig. 4. The data are consistent with the value of γ indicated by previous measurements [4, 5], $\sim 70^\circ$, and result in a value of $r_B = 0.11 \pm 0.02$. This value of r_B is determined at the point where the global χ^2 of the fit is minimised.

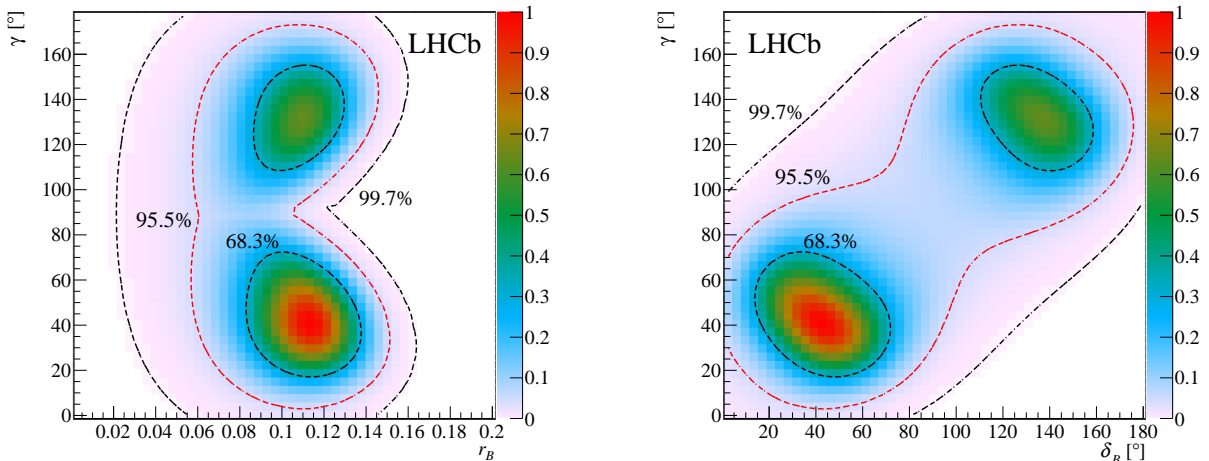


Figure 4: Contour plots showing 2D scans of physics parameters γ versus r_B (left) and γ versus δ_B (right). The dashed lines represent the $\Delta\chi^2 = 2.30, 6.18, 11.8$ contours, corresponding to 68.3%, 95.5%, 99.7% confidence levels (CL), respectively. The colour scale represents $1 - \text{CL}$.

7 Conclusions

A study of the $B^- \rightarrow DK^{*-}$ decay mode is presented where the D meson decays to two- and four-body final states consisting of charged kaons and/or pions. The CP observables R_{CP+} , A_{CP+} , $R_{K\pi}^+$, $R_{K\pi}^-$, $R_{\pi\pi\pi\pi}$, $A_{\pi\pi\pi\pi}$, $R_{K\pi\pi\pi}^+$ and $R_{K\pi\pi\pi}^-$ are measured from the high purity sample obtained from pp collision data recorded with the LHCb detector in Run 1 and Run 2. The measurement of the CP asymmetries in the two-body decay modes and their ratio to the favoured decay mode is consistent with and more precise than the previous determination [16]. While no bounds on γ are quoted due to the limited sensitivity of this decay mode in isolation, $B^- \rightarrow DK^{*-}$ decays will become valuable in constraining γ in the future, as more data are collected and more D decay modes are analysed.

Acknowledgements

We express our gratitude to our colleagues in the CERN accelerator departments for the excellent performance of the LHC. We thank the technical and administrative staff at the LHCb institutes. We acknowledge support from CERN and from the national agencies: CAPES, CNPq, FAPERJ and FINEP (Brazil); MOST and NSFC (China); CNRS/IN2P3 (France); BMBF, DFG and MPG (Germany); INFN (Italy); NWO (The Netherlands); MNiSW and NCN (Poland); MEN/IFA (Romania); MinES and FASO (Russia); MinECo (Spain); SNSF and SER (Switzerland); NASU (Ukraine); STFC (United Kingdom); NSF (USA). We acknowledge the computing resources that are provided by CERN, IN2P3 (France), KIT and DESY (Germany), INFN (Italy), SURF (The Netherlands), PIC (Spain), GridPP (United Kingdom), RRCKI and Yandex LLC (Russia), CSCS (Switzerland), IFIN-HH (Romania), CBPF (Brazil), PL-GRID (Poland) and OSC (USA). We are indebted to the communities behind the multiple open-source software packages on which we depend. Individual groups or members have received support from AvH Foundation (Germany), EPLANET, Marie Skłodowska-Curie Actions and ERC (European Union), ANR, Labex P2IO, ENIGMASS and OCEVU, and Région Auvergne-Rhône-Alpes (France), RFBR and Yandex LLC (Russia), GVA, XuntaGal and GENCAT (Spain), Herchel Smith Fund, the Royal Society, the English-Speaking Union and the Leverhulme Trust (United Kingdom).

References

- [1] N. Cabibbo, *Unitary symmetry and leptonic decays*, Phys. Rev. Lett. **10** (1963) 531.
- [2] M. Kobayashi and T. Maskawa, *CP violation in the renormalizable theory of weak interaction*, Progress of Theoretical Physics **49** (1973) 652.
- [3] C. Jarlskog, *Commutator of the quark mass matrices in the standard electroweak model and a measure of maximal CP nonconservation*, Phys. Rev. Lett. **55** (1985) 1039.
- [4] LHCb collaboration, R. Aaij *et al.*, *Measurement of the CKM angle γ from a combination of LHCb results*, JHEP **12** (2016) 087, [arXiv:1611.03076](https://arxiv.org/abs/1611.03076).
- [5] CKMfitter group, J. Charles *et al.*, *CP violation and the CKM matrix: Assessing the impact of the asymmetric B factories*, Eur. Phys. J. **C41** (2005) 1, [arXiv:hep-ph/0406184](https://arxiv.org/abs/hep-ph/0406184), updated results and plots available at: <http://ckmfitter.in2p3.fr>.
- [6] LHCb collaboration, R. Aaij *et al.*, *Measurement of CP observables in $B^\pm \rightarrow DK^\pm$ and $B^\pm \rightarrow D\pi^\pm$ with two- and four-body D decays*, Phys. Lett. **B760** (2016) 117, [arXiv:1603.08993](https://arxiv.org/abs/1603.08993).
- [7] LHCb collaboration, R. Aaij *et al.*, *Measurement of the CKM angle γ using $B^\pm \rightarrow DK^\pm$ with $D \rightarrow K_s^0\pi^+\pi^-$, $K_s^0K^+K^-$ decays*, JHEP **10** (2014) 097, [arXiv:1408.2748](https://arxiv.org/abs/1408.2748).
- [8] LHCb collaboration, R. Aaij *et al.*, *A study of CP violation in $B^\mp \rightarrow Dh^\mp$ ($h = K, \pi$) with the modes $D \rightarrow K^\mp\pi^\pm\pi^0$, $D \rightarrow \pi^+\pi^-\pi^0$ and $D \rightarrow K^+K^-\pi^0$* , Phys. Rev. **D91** (2015) 112014, [arXiv:1504.05442](https://arxiv.org/abs/1504.05442).

- [9] M. Gronau and D. London, *How to determine all the angles of the unitarity triangle from $B_d^0 \rightarrow DK_S$ and $B_s^0 \rightarrow D\phi$* , Phys. Lett. **B253** (1991) 483.
- [10] M. Gronau and D. Wyler, *On determining a weak phase from charged B decay asymmetries*, Phys. Lett. **B265** (1991) 172.
- [11] D. Atwood, I. Dunietz, and A. Soni, *Enhanced CP violation with $B \rightarrow KD^0(\bar{D}^0)$ modes and extraction of the Cabibbo-Kobayashi-Maskawa angle γ* , Phys. Rev. Lett. **78** (1997) 3257.
- [12] D. Atwood, I. Dunietz, and A. Soni, *Improved methods for observing CP violation in $B^\pm \rightarrow KD$ and measuring the CKM phase γ* , Phys. Rev. **D63** (2001) 036005, arXiv:hep-ph/0008090.
- [13] LHCb collaboration, R. Aaij *et al.*, *Measurement of CP violation parameters in $B^0 \rightarrow DK^{*0}$ decays*, Phys. Rev. **D90** (2014) 112002, arXiv:1407.8136.
- [14] D. Atwood and A. Soni, *Role of a charm factory in extracting CKM-phase information via $B \rightarrow DK$* , Phys. Rev. **D68** (2003) 033003, arXiv:hep-ph/0304085.
- [15] S. Malde *et al.*, *First determination of the CP content of $D \rightarrow \pi^+\pi^-\pi^+\pi^-$ and updated determination of the CP contents of $D \rightarrow \pi^+\pi^-\pi^0$ and $D \rightarrow K^+K^-\pi^0$* , Phys. Lett. **B747** (2015) 9, arXiv:1504.05878.
- [16] BaBar collaboration, B. Aubert *et al.*, *Measurement of CP violation observables and parameters for the decays $B^\pm \rightarrow DK^{*\pm}$* , Phys. Rev. **D80** (2009) 092001, arXiv:0909.3981.
- [17] BaBar collaboration, B. Aubert *et al.*, *Improved measurement of the CKM angle γ in $B^\mp \rightarrow D^{(*)}K^{(*)\mp}$ decays with a Dalitz plot analysis of D decays to $K_S^0\pi^+\pi^-$ and $K_S^0K^+K^-$* , Phys. Rev. **D78** (2008) 034023, arXiv:0804.2089.
- [18] Belle collaboration, A. Poluektov *et al.*, *Measurement of ϕ_3 with a Dalitz plot analysis of $B^+ \rightarrow D^{(*)}K^{(*)+}$ decay*, Phys. Rev. **D73** (2006) 112009, arXiv:hep-ex/0604054.
- [19] W. Wang, *CP violation effects on the measurement of the Cabibbo-Kobayashi-Maskawa angle γ from $B \rightarrow DK$* , Phys. Rev. Lett. **110** (2013) 061802, arXiv:1211.4539.
- [20] M. Gronau, *Improving bounds on γ in $B^\pm \rightarrow DK^{*\pm}$ and $B^{\pm,0} \rightarrow DX_s^{\pm,0}$* , Phys. Lett. **B557** (2003) 198.
- [21] M. Rama, *Effect of $D - \bar{D}$ mixing in the extraction of γ with $B^- \rightarrow D^0K^-$ and $B^- \rightarrow D^0\pi^-$ decays*, Phys. Rev. **D89** (2014) 014021, arXiv:1307.4384.
- [22] Heavy Flavor Averaging Group, Y. Amhis *et al.*, *Averages of b -hadron, c -hadron, and τ -lepton properties as of summer 2016*, arXiv:1612.07233, updated results and plots available at <http://www.slac.stanford.edu/xorg/hflav/>.
- [23] T. Evans *et al.*, *Improved determination of the $D \rightarrow K^+\pi^-\pi^+\pi^-$ coherence factor and associated hadronic parameters from a combination of $e^+e^- \rightarrow \Upsilon(3770) \rightarrow c\bar{c}$ and $pp \rightarrow c\bar{c}X$ data*, Phys. Lett. **B757** (2016) 520, Corrigendum *ibid.* **B765** (2017) 402, arXiv:1602.07430.

- [24] LHCb collaboration, R. Aaij *et al.*, *First observation of $D^0 - \bar{D}^0$ oscillations in $D^0 \rightarrow K^+\pi^+\pi^-\pi^-$ decays and a measurement of the associated coherence parameters*, Phys. Rev. Lett. **116** (2016) 241801, [arXiv:1602.07224](#).
- [25] LHCb collaboration, A. A. Alves Jr. *et al.*, *The LHCb detector at the LHC*, JINST **3** (2008) S08005.
- [26] LHCb collaboration, R. Aaij *et al.*, *LHCb detector performance*, Int. J. Mod. Phys. **A30** (2015) 1530022, [arXiv:1412.6352](#).
- [27] R. Aaij *et al.*, *The LHCb trigger and its performance in 2011*, JINST **8** (2013) P04022, [arXiv:1211.3055](#).
- [28] V. V. Gligorov and M. Williams, *Efficient, reliable and fast high-level triggering using a bonsai boosted decision tree*, JINST **8** (2013) P02013, [arXiv:1210.6861](#).
- [29] LHCb collaboration, R. Aaij *et al.*, *Measurement of forward J/ψ production cross-sections in pp collisions at $\sqrt{s} = 13$ TeV*, JHEP **10** (2015) 172, Erratum *ibid.* **05** (2017) 063, [arXiv:1509.00771](#).
- [30] M. Adinolfi *et al.*, *Performance of the LHCb RICH detector at the LHC*, Eur. Phys. J. **C73** (2013) 2431, [arXiv:1211.6759](#).
- [31] T. Sjöstrand, S. Mrenna, and P. Skands, *PYTHIA 6.4 physics and manual*, JHEP **05** (2006) 026, [arXiv:hep-ph/0603175](#); T. Sjöstrand, S. Mrenna, and P. Skands, *A brief introduction to PYTHIA 8.1*, Comput. Phys. Commun. **178** (2008) 852, [arXiv:0710.3820](#).
- [32] I. Belyaev *et al.*, *Handling of the generation of primary events in Gauss, the LHCb simulation framework*, J. Phys. Conf. Ser. **331** (2011) 032047.
- [33] D. J. Lange, *The EvtGen particle decay simulation package*, Nucl. Instrum. Meth. **A462** (2001) 152.
- [34] P. Golonka and Z. Was, *PHOTOS Monte Carlo: A precision tool for QED corrections in Z and W decays*, Eur. Phys. J. **C45** (2006) 97, [arXiv:hep-ph/0506026](#).
- [35] Geant4 collaboration, J. Allison *et al.*, *Geant4 developments and applications*, IEEE Trans. Nucl. Sci. **53** (2006) 270; Geant4 collaboration, S. Agostinelli *et al.*, *Geant4: A simulation toolkit*, Nucl. Instrum. Meth. **A506** (2003) 250.
- [36] M. Clemencic *et al.*, *The LHCb simulation application, Gauss: Design, evolution and experience*, J. Phys. Conf. Ser. **331** (2011) 032023.
- [37] Particle Data Group, C. Patrignani *et al.*, *Review of particle physics*, Chin. Phys. **C40** (2016) 100001.
- [38] W. D. Hulsbergen, *Decay chain fitting with a Kalman filter*, Nucl. Instrum. Meth. **A552** (2005) 566, [arXiv:physics/0503191](#).
- [39] L. Breiman, J. H. Friedman, R. A. Olshen, and C. J. Stone, *Classification and regression trees*, Wadsworth international group, Belmont, California, USA, 1984.

- [40] T. Skwarnicki, *A study of the radiative cascade transitions between the Upsilon-prime and Upsilon resonances*, PhD thesis, Institute of Nuclear Physics, Krakow, 1986, DESY-F31-86-02.
- [41] LHCb collaboration, R. Aaij *et al.*, *Measurement of CP observables in $B^\pm \rightarrow D^{(*)}K^\pm$ and $B^\pm \rightarrow D^{(*)}\pi^\pm$ decays*, arXiv:1708.06370, submitted to Phys. Lett. B.
- [42] LHCb collaboration, R. Aaij *et al.*, *Model-independent measurement of the CKM angle γ using $B^0 \rightarrow DK^{*0}$ decays with $D \rightarrow K_s^0\pi^+\pi^-$ and $K_s^0K^+K^-$* , JHEP **06** (2016) 131, arXiv:1604.01525.
- [43] LHCb collaboration, R. Aaij *et al.*, *Measurement of the B^\pm production asymmetry and the CP asymmetry in $B^\pm \rightarrow J/\psi K^\pm$ decays*, Phys. Rev. **D95** (2017) 052005, arXiv:1701.05501.
- [44] LHCb collaboration, R. Aaij *et al.*, *Measurement of CP asymmetry in $D^0 \rightarrow K^-K^+$ and $D^0 \rightarrow \pi^-\pi^+$ decays*, JHEP **07** (2014) 041, arXiv:1405.2797.
- [45] LHCb collaboration, R. Aaij *et al.*, *Measurement of the $D_s^+ - D_s^-$ production asymmetry in 7 TeV pp collisions*, Phys. Lett. **B713** (2012) 186, arXiv:1205.0897.
- [46] S. S. Wilks, *The large-sample distribution of the likelihood ratio for testing composite hypotheses*, Ann. Math. Stat. **9** (1938) 60.
- [47] LHCb collaboration, R. Aaij *et al.*, *Dalitz plot analysis of $B_s^0 \rightarrow \bar{D}^0 K^- \pi^+$ decays*, Phys. Rev. **D90** (2014) 072003, arXiv:1407.7712.
- [48] T. Latham, J. Back, and P. Harrison, *Laura++*, a Dalitz plot fitting package, available at <https://laura.hepforge.org/>.
- [49] D. Aston *et al.*, *A study of $K^-\pi^+$ scattering in the reaction $K^-p \rightarrow K^-\pi^+n$ at 11 GeV/c*, Nucl. Phys. **B296** (1988) 493.

LHCb collaboration

R. Aaij⁴⁰, B. Adeva³⁹, M. Adinolfi⁴⁸, Z. Ajaltouni⁵, S. Akar⁵⁹, J. Albrecht¹⁰, F. Alessio⁴⁰, M. Alexander⁵³, A. Alfonso Alberio³⁸, S. Ali⁴³, G. Alkhazov³¹, P. Alvarez Cartelle⁵⁵, A.A. Alves Jr⁵⁹, S. Amato², S. Amerio²³, Y. Amhis⁷, L. An³, L. Anderlini¹⁸, G. Andreassi⁴¹, M. Andreotti^{17,g}, J.E. Andrews⁶⁰, R.B. Appleby⁵⁶, F. Archilli⁴³, P. d'Argent¹², J. Arnau Romeu⁶, A. Artamonov³⁷, M. Artuso⁶¹, E. Aslanides⁶, M. Atzeni⁴², G. Auremma²⁶, M. Baalouch⁵, I. Babuschkin⁵⁶, S. Bachmann¹², J.J. Back⁵⁰, A. Badalov^{38,m}, C. Baesso⁶², S. Baker⁵⁵, V. Balagura^{7,b}, W. Baldini¹⁷, A. Baranov³⁵, R.J. Barlow⁵⁶, C. Barschel⁴⁰, S. Barsuk⁷, W. Barter⁵⁶, F. Baryshnikov³², V. Batozskaya²⁹, V. Battista⁴¹, A. Bay⁴¹, L. Beaucourt⁴, J. Beddow⁵³, F. Bedeschi²⁴, I. Bediaga¹, A. Beiter⁶¹, L.J. Bel⁴³, N. Belyi⁶³, V. Bellee⁴¹, N. Belloli^{21,i}, K. Belous³⁷, I. Belyaev^{32,40}, E. Ben-Haim⁸, G. Bencivenni¹⁹, S. Benson⁴³, S. Beranek⁹, A. Berezhnoy³³, R. Bernet⁴², D. Berninghoff¹², E. Bertholet⁸, A. Bertolin²³, C. Betancourt⁴², F. Betti¹⁵, M.-O. Bettler⁴⁰, M. van Beuzekom⁴³, I.a. Bezshyiko⁴², S. Bifani⁴⁷, P. Billoir⁸, A. Birnkraut¹⁰, A. Bizzeti^{18,u}, M. Bjørn⁵⁷, T. Blake⁵⁰, F. Blanc⁴¹, S. Blusk⁶¹, V. Bocci²⁶, T. Boettcher⁵⁸, A. Bondar^{36,w}, N. Bondar³¹, I. Bordyuzhin³², A. Borgheresi^{21,i}, S. Borghi⁵⁶, M. Borisyak³⁵, M. Borsato³⁹, F. Bossu⁷, M. Boubdir⁹, T.J.V. Bowcock⁵⁴, E. Bowen⁴², C. Bozzi^{17,40}, S. Braun¹², T. Britton⁶¹, J. Brodzicka²⁷, D. Brundu¹⁶, E. Buchanan⁴⁸, C. Buri⁵⁶, A. Bursche^{16,f}, J. Buytaert⁴⁰, W. Byczynski⁴⁰, S. Cadeddu¹⁶, H. Cai⁶⁴, R. Calabrese^{17,g}, R. Calladine⁴⁷, M. Calvi^{21,i}, M. Calvo Gomez^{38,m}, A. Camboni^{38,m}, P. Campana¹⁹, D.H. Campora Perez⁴⁰, L. Capriotti⁵⁶, A. Carbone^{15,e}, G. Carboni^{25,j}, R. Cardinale^{20,h}, A. Cardini¹⁶, P. Carniti^{21,i}, L. Carson⁵², K. Carvalho Akiba², G. Casse⁵⁴, L. Cassina²¹, M. Cattaneo⁴⁰, G. Cavallero^{20,40,h}, R. Cenci^{24,t}, D. Chamont⁷, M.G. Chapman⁴⁸, M. Charles⁸, Ph. Charpentier⁴⁰, G. Chatzikonstantinidis⁴⁷, M. Chefdeville⁴, S. Chen¹⁶, S.F. Cheung⁵⁷, S.-G. Chitic⁴⁰, V. Chobanova^{39,40}, M. Chruszcz^{42,27}, A. Chubykin³¹, P. Ciambone¹⁹, X. Cid Vidal³⁹, G. Ciezarek⁴³, P.E.L. Clarke⁵², M. Clemencic⁴⁰, H.V. Cliff⁴⁹, J. Closier⁴⁰, J. Cogan⁶, E. Cogneras⁵, V. Cogoni^{16,f}, L. Cojocariu³⁰, P. Collins⁴⁰, T. Colombo⁴⁰, A. Comerma-Montells¹², A. Contu⁴⁰, A. Cook⁴⁸, G. Coombs⁴⁰, S. Coquereau³⁸, G. Corti⁴⁰, M. Corvo^{17,g}, C.M. Costa Sobral⁵⁰, B. Couturier⁴⁰, G.A. Cowan⁵², D.C. Craik⁵⁸, A. Crocombe⁵⁰, M. Cruz Torres¹, R. Currie⁵², C. D'Ambrosio⁴⁰, F. Da Cunha Marinho², E. Dall'Occo⁴³, J. Dalseno⁴⁸, A. Davis³, O. De Aguiar Francisco⁴⁰, S. De Capua⁵⁶, M. De Cian¹², J.M. De Miranda¹, L. De Paula², M. De Serio^{14,d}, P. De Simone¹⁹, C.T. Dean⁵³, D. Decamp⁴, L. Del Buono⁸, H.-P. Dembinski¹¹, M. Demmer¹⁰, A. Dendek²⁸, D. Derkach³⁵, O. Deschamps⁵, F. Dettori⁵⁴, B. Dey⁶⁵, A. Di Canto⁴⁰, P. Di Nezza¹⁹, H. Dijkstra⁴⁰, F. Dordei⁴⁰, M. Dorigo⁴⁰, A. Dosil Suárez³⁹, L. Douglas⁵³, A. Dovbnya⁴⁵, K. Dreimanis⁵⁴, L. Dufour⁴³, G. Dujany⁸, P. Durante⁴⁰, R. Dzhelyadin³⁷, M. Dziewiecki¹², A. Dziurda⁴⁰, A. Dzyuba³¹, S. Easo⁵¹, M. Ebert⁵², U. Egede⁵⁵, V. Egorychev³², S. Eidelman^{36,w}, S. Eisenhardt⁵², U. Eitschberger¹⁰, R. Ekelhof¹⁰, L. Eklund⁵³, S. Ely⁶¹, S. Esen¹², H.M. Evans⁴⁹, T. Evans⁵⁷, A. Falabella¹⁵, N. Farley⁴⁷, S. Farry⁵⁴, D. Fazzini^{21,i}, L. Federici²⁵, D. Ferguson⁵², G. Fernandez³⁸, P. Fernandez Declara⁴⁰, A. Fernandez Prieto³⁹, F. Ferrari¹⁵, F. Ferreira Rodrigues², M. Ferro-Luzzi⁴⁰, S. Filippov³⁴, R.A. Fini¹⁴, M. Fiorini^{17,g}, M. Firlej²⁸, C. Fitzpatrick⁴¹, T. Fiutowski²⁸, F. Fleuret^{7,b}, K. Fohl⁴⁰, M. Fontana^{16,40}, F. Fontanelli^{20,h}, D.C. Forshaw⁶¹, R. Forty⁴⁰, V. Franco Lima⁵⁴, M. Frank⁴⁰, C. Frei⁴⁰, J. Fu^{22,q}, W. Funk⁴⁰, E. Furfaro^{25,j}, C. Färber⁴⁰, E. Gabriel⁵², A. Gallas Torreira³⁹, D. Galli^{15,e}, S. Gallorini²³, S. Gambetta⁵², M. Gandelman², P. Gandini²², Y. Gao³, L.M. Garcia Martin⁷⁰, J. García Pardiñas³⁹, J. Garra Tico⁴⁹, L. Garrido³⁸, P.J. Garsed⁴⁹, D. Gascon³⁸, C. Gaspar⁴⁰, L. Gavardi¹⁰, G. Gazzoni⁵, D. Gerick¹², E. Gersabeck¹², M. Gersabeck⁵⁶, T. Gershon⁵⁰, Ph. Ghez⁴, S. Gianì⁴¹, V. Gibson⁴⁹, O.G. Girard⁴¹, L. Giubega³⁰, K. Gizdov⁵², V.V. Gligorov⁸, D. Golubkov³², A. Golutvin⁵⁵, A. Gomes^{1,a}, I.V. Gorelov³³, C. Gotti^{21,i}, E. Govorkova⁴³, J.P. Grabowski¹², R. Graciani Diaz³⁸, L.A. Granado Cardoso⁴⁰, E. Graugés³⁸, E. Graverini⁴²,

G. Graziani¹⁸, A. Grecu³⁰, R. Greim⁹, P. Griffith¹⁶, L. Grillo²¹, L. Gruber⁴⁰,
 B.R. Gruberg Cazon⁵⁷, O. Grünberg⁶⁷, E. Gushchin³⁴, Yu. Guz³⁷, T. Gys⁴⁰, C. Göbel⁶²,
 T. Hadavizadeh⁵⁷, C. Hadjivasiliou⁵, G. Haefeli⁴¹, C. Haen⁴⁰, S.C. Haines⁴⁹, B. Hamilton⁶⁰,
 X. Han¹², T.H. Hancock⁵⁷, S. Hansmann-Menzemer¹², N. Harnew⁵⁷, S.T. Harnew⁴⁸, C. Hasse⁴⁰,
 M. Hatch⁴⁰, J. He⁶³, M. Hecker⁵⁵, K. Heinicke¹⁰, A. Heister⁹, K. Hennessy⁵⁴, P. Henrard⁵,
 L. Henry⁷⁰, E. van Herwijnen⁴⁰, M. Heß⁶⁷, A. Hicheur², D. Hill⁵⁷, C. Hombach⁵⁶,
 P.H. Hopchev⁴¹, W. Hu⁶⁵, Z.C. Huard⁵⁹, W. Hulsbergen⁴³, T. Humair⁵⁵, M. Hushchyn³⁵,
 D. Hutchcroft⁵⁴, P. Ibis¹⁰, M. Idzik²⁸, P. Ilten⁵⁸, R. Jacobsson⁴⁰, J. Jalocha⁵⁷, E. Jans⁴³,
 A. Jawahery⁶⁰, F. Jiang³, M. John⁵⁷, D. Johnson⁴⁰, C.R. Jones⁴⁹, C. Joram⁴⁰, B. Jost⁴⁰,
 N. Jurik⁵⁷, S. Kandybei⁴⁵, M. Karacson⁴⁰, J.M. Kariuki⁴⁸, S. Karodia⁵³, N. Kazeev³⁵,
 M. Kecke¹², F. Keizer⁴⁹, M. Kelsey⁶¹, M. Kenzie⁴⁹, T. Ketel⁴⁴, E. Khairullin³⁵, B. Khanji¹²,
 C. Khurewathanakul⁴¹, T. Kirn⁹, S. Klaver⁵⁶, K. Klimaszewski²⁹, T. Klimovich¹¹, S. Koliiev⁴⁶,
 M. Kolpin¹², I. Komarov⁴¹, R. Kopečna¹², P. Koppenburg⁴³, A. Kosmyntseva³²,
 S. Kotriakhova³¹, M. Kozeiha⁵, L. Kravchuk³⁴, M. Kreps⁵⁰, F. Kress⁵⁵, P. Krokovny^{36,w},
 F. Kruse¹⁰, W. Krzemien²⁹, W. Kucewicz^{27,l}, M. Kucharczyk²⁷, V. Kudryavtsev^{36,w},
 A.K. Kuonen⁴¹, T. Kvaratskheliya^{32,40}, D. Lacarrere⁴⁰, G. Lafferty⁵⁶, A. Lai¹⁶, G. Lanfranchi¹⁹,
 C. Langenbruch⁹, T. Latham⁵⁰, C. Lazzeroni⁴⁷, R. Le Gac⁶, A. Leflat^{33,40}, J. Lefrançois⁷,
 R. Lefèvre⁵, F. Lemaitre⁴⁰, E. Lemos Cid³⁹, O. Leroy⁶, T. Lesiak²⁷, B. Leverington¹²,
 P.-R. Li⁶³, T. Li³, Y. Li⁷, Z. Li⁶¹, T. Likhomanenko⁶⁸, R. Lindner⁴⁰, F. Lionetto⁴²,
 V. Lisovskyi⁷, X. Liu³, D. Loh⁵⁰, A. Loi¹⁶, I. Longstaff⁵³, J.H. Lopes², D. Lucchesi^{23,o},
 M. Lucio Martinez³⁹, H. Luo⁵², A. Lupato²³, E. Luppi^{17,g}, O. Lupton⁴⁰, A. Lusiani²⁴, X. Lyu⁶³,
 F. Machefert⁷, F. Maciuc³⁰, V. Macko⁴¹, P. Mackowiak¹⁰, S. Maddrell-Mander⁴⁸, O. Maev^{31,40},
 K. Maguire⁵⁶, D. Maisuzenko³¹, M.W. Majewski²⁸, S. Malde⁵⁷, B. Malecki²⁷, A. Malinin⁶⁸,
 T. Maltsev^{36,w}, G. Manca^{16,f}, G. Mancinelli⁶, D. Marangotto^{22,q}, J. Maratas^{5,v},
 J.F. Marchand⁴, U. Marconi¹⁵, C. Marin Benito³⁸, M. Marinangeli⁴¹, P. Marino⁴¹, J. Marks¹²,
 G. Martellotti²⁶, M. Martin⁶, M. Martinelli⁴¹, D. Martinez Santos³⁹, F. Martinez Vidal⁷⁰,
 D. Martins Tostes², L.M. Massacrier⁷, A. Massafferri¹, R. Matev⁴⁰, A. Mathad⁵⁰, Z. Mathe⁴⁰,
 C. Matteuzzi²¹, A. Mauri⁴², E. Maurice^{7,b}, B. Maurin⁴¹, A. Mazurov⁴⁷, M. McCann^{55,40},
 A. McNab⁵⁶, R. McNulty¹³, J.V. Mead⁵⁴, B. Meadows⁵⁹, C. Meaux⁶, F. Meier¹⁰, N. Meinert⁶⁷,
 D. Melnychuk²⁹, M. Merk⁴³, A. Merli^{22,40,q}, E. Michielin²³, D.A. Milanese⁶⁶, E. Millard⁵⁰,
 M.-N. Minard⁴, L. Minzoni¹⁷, D.S. Mitzel¹², A. Mogini⁸, J. Molina Rodriguez¹,
 T. Mombächer¹⁰, I.A. Monroy⁶⁶, S. Monteil⁵, M. Morandin²³, M.J. Morello^{24,t}, O. Morgunova⁶⁸,
 J. Moron²⁸, A.B. Morris⁵², R. Mountain⁶¹, F. Muheim⁵², M. Mulder⁴³, D. Müller⁵⁶, J. Müller¹⁰,
 K. Müller⁴², V. Müller¹⁰, P. Naik⁴⁸, T. Nakada⁴¹, R. Nandakumar⁵¹, A. Nandi⁵⁷, I. Nasteva²,
 M. Needham⁵², N. Neri^{22,40}, S. Neubert¹², N. Neufeld⁴⁰, M. Neuner¹², T.D. Nguyen⁴¹,
 C. Nguyen-Mau^{41,n}, S. Nieswand⁹, R. Niet¹⁰, N. Nikitin³³, T. Nikodem¹², A. Nogay⁶⁸,
 D.P. O’Hanlon⁵⁰, A. Oblakowska-Mucha²⁸, V. Obraztsov³⁷, S. Ogilvy¹⁹, R. Oldeman^{16,f},
 C.J.G. Onderwater⁷¹, A. Ossowska²⁷, J.M. Otalora Goicochea², P. Owen⁴², A. Oyanguren⁷⁰,
 P.R. Pais⁴¹, A. Palano^{14,d}, M. Palutan^{19,40}, A. Papanestis⁵¹, M. Pappagallo^{14,d},
 L.L. Pappalardo^{17,g}, W. Parker⁶⁰, C. Parkes⁵⁶, G. Passaleva^{18,40}, A. Pastore^{14,d}, M. Patel⁵⁵,
 C. Patrignani^{15,e}, A. Pearce⁴⁰, A. Pellegrino⁴³, G. Penso²⁶, M. Pepe Altarelli⁴⁰, S. Perazzini⁴⁰,
 P. Perret⁵, L. Pescatore⁴¹, K. Petridis⁴⁸, A. Petrolini^{20,h}, A. Petrov⁶⁸, M. Petruzzo^{22,q},
 E. Picatoste Olloqui³⁸, B. Pietrzyk⁴, M. Piekies²⁷, D. Pinci²⁶, F. Pisani⁴⁰, A. Pistone^{20,h},
 A. Piucci¹², V. Placinta³⁰, S. Playfer⁵², M. Plo Casasus³⁹, F. Polci⁸, M. Poli Lener¹⁹,
 A. Poluektov⁵⁰, I. Polyakov⁶¹, E. Polcarpo², G.J. Pomery⁴⁸, S. Ponce⁴⁰, A. Popov³⁷,
 D. Popov^{11,40}, S. Poslavskii³⁷, C. Potterat², E. Price⁴⁸, J. Prisciandaro³⁹, C. Prouve⁴⁸,
 V. Pugatch⁴⁶, A. Puig Navarro⁴², H. Pullen⁵⁷, G. Punzi^{24,p}, W. Qian⁵⁰, R. Quagliani^{7,48},
 B. Quintana⁵, B. Rachwal²⁸, J.H. Rademacker⁴⁸, M. Rama²⁴, M. Ramos Pernas³⁹,
 M.S. Rangel², I. Raniuk^{45,†}, F. Ratnikov³⁵, G. Raven⁴⁴, M. Ravonel Salzgeber⁴⁰, M. Reboud⁴,
 F. Redi⁵⁵, S. Reichert¹⁰, A.C. dos Reis¹, C. Remon Alepuz⁷⁰, V. Renaudin⁷, S. Ricciardi⁵¹,

S. Richards⁴⁸, M. Rihl⁴⁰, K. Rinnert⁵⁴, V. Rives Molina³⁸, P. Robbe⁷, A. Robert⁸,
A.B. Rodrigues¹, E. Rodrigues⁵⁹, J.A. Rodriguez Lopez⁶⁶, A. Rogozhnikov³⁵, S. Roiser⁴⁰,
A. Rollings⁵⁷, V. Romanovskiy³⁷, A. Romero Vidal³⁹, J.W. Ronayne¹³, M. Rotondo¹⁹,
M.S. Rudolph⁶¹, T. Ruf⁴⁰, P. Ruiz Valls⁷⁰, J. Ruiz Vidal⁷⁰, J.J. Saborido Silva³⁹,
E. Sadykhov³², N. Sagidova³¹, B. Saitta^{16,f}, V. Salustino Guimaraes¹,
C. Sanchez Mayordomo⁷⁰, B. Sanmartin Sedes³⁹, R. Santacesaria²⁶, C. Santamarina Rios³⁹,
M. Santimaria¹⁹, E. Santovetti^{25,j}, G. Sarpis⁵⁶, A. Sarti^{19,k}, C. Satriano^{26,s}, A. Satta²⁵,
D.M. Saunders⁴⁸, D. Savrina^{32,33}, S. Schael⁹, M. Schellenberg¹⁰, M. Schiller⁵³, H. Schindler⁴⁰,
M. Schmelling¹¹, T. Schmelzer¹⁰, B. Schmidt⁴⁰, O. Schneider⁴¹, A. Schopper⁴⁰, H.F. Schreiner⁵⁹,
M. Schubiger⁴¹, M.-H. Schune⁷, R. Schwemmer⁴⁰, B. Sciascia¹⁹, A. Sciubba^{26,k},
A. Semennikov³², E.S. Sepulveda⁸, A. Sergi⁴⁷, N. Serra⁴², J. Serrano⁶, L. Sestini²³, P. Seyfert⁴⁰,
M. Shapkin³⁷, I. Shapoval⁴⁵, Y. Shcheglov³¹, T. Shears⁵⁴, L. Shekhtman^{36,w}, V. Shevchenko⁶⁸,
B.G. Siddi¹⁷, R. Silva Coutinho⁴², L. Silva de Oliveira², G. Simi^{23,o}, S. Simone^{14,d}, M. Sirendi⁴⁹,
N. Skidmore⁴⁸, T. Skwarnicki⁶¹, E. Smith⁵⁵, I.T. Smith⁵², J. Smith⁴⁹, M. Smith⁵⁵,
I. Soares Lavra¹, M.D. Sokoloff⁵⁹, F.J.P. Soler⁵³, B. Souza De Paula², B. Spaan¹⁰, P. Spradlin⁵³,
S. Sridharan⁴⁰, F. Stagni⁴⁰, M. Stahl¹², S. Stahl⁴⁰, P. Stefko⁴¹, S. Stefkova⁵⁵, O. Steinkamp⁴²,
S. Stemmler¹², O. Stenyakin³⁷, M. Stepanova³¹, H. Stevens¹⁰, S. Stone⁶¹, B. Storaci⁴²,
S. Stracka^{24,p}, M.E. Stramaglia⁴¹, M. Straticiu³⁰, U. Straumann⁴², J. Sun³, L. Sun⁶⁴,
W. Sutcliffe⁵⁵, K. Swientek²⁸, V. Syropoulos⁴⁴, T. Szumlak²⁸, M. Szymanski⁶³, S. T'Jampens⁴,
A. Tayduganov⁶, T. Tekampe¹⁰, G. Tellarini^{17,g}, F. Teubert⁴⁰, E. Thomas⁴⁰, J. van Tilburg⁴³,
M.J. Tilley⁵⁵, V. Tisserand⁴, M. Tobin⁴¹, S. Tol⁴⁹, L. Tomassetti^{17,g}, D. Tonelli²⁴, F. Toriello⁶¹,
R. Tourinho Jadallah Aoude¹, E. Tournefier⁴, M. Traill⁵³, M.T. Tran⁴¹, M. Tresch⁴²,
A. Trisovic⁴⁰, A. Tsaregorodtsev⁶, P. Tsopelas⁴³, A. Tully⁴⁹, N. Tuning^{43,40}, A. Ukleja²⁹,
A. Usachov⁷, A. Ustyuzhanin³⁵, U. Uwer¹², C. Vacca^{16,f}, A. Vagner⁶⁹, V. Vagnoni^{15,40},
A. Valassi⁴⁰, S. Valat⁴⁰, G. Valenti¹⁵, R. Vazquez Gomez⁴⁰, P. Vazquez Regueiro³⁹, S. Vecchi¹⁷,
M. van Veghel⁴³, J.J. Velthuis⁴⁸, M. Veltri^{18,r}, G. Veneziano⁵⁷, A. Venkateswaran⁶¹,
T.A. Verlage⁹, M. Vernet⁵, M. Vesterinen⁵⁷, J.V. Viana Barbosa⁴⁰, B. Viaud⁷, D. Vieira⁶³,
M. Vieites Diaz³⁹, H. Viemann⁶⁷, X. Vilasis-Cardona^{38,m}, M. Vitti⁴⁹, V. Volkov³³,
A. Vollhardt⁴², B. Voneki⁴⁰, A. Vorobyev³¹, V. Vorobyev^{36,w}, C. Voß⁹, J.A. de Vries⁴³,
C. Vázquez Sierra³⁹, R. Waldi⁶⁷, C. Wallace⁵⁰, R. Wallace¹³, J. Walsh²⁴, J. Wang⁶¹,
D.R. Ward⁴⁹, H.M. Wark⁵⁴, N.K. Watson⁴⁷, D. Websdale⁵⁵, A. Weiden⁴², C. Weisser⁵⁸,
M. Whitehead⁴⁰, J. Wicht⁵⁰, G. Wilkinson⁵⁷, M. Wilkinson⁶¹, M. Williams⁵⁶, M.P. Williams⁴⁷,
M. Williams⁵⁸, T. Williams⁴⁷, F.F. Wilson^{51,40}, J. Wimberley⁶⁰, M. Winn⁷, J. Wishahi¹⁰,
W. Wislicki²⁹, M. Witek²⁷, G. Wormser⁷, S.A. Wotton⁴⁹, K. Wraight⁵³, K. Wyllie⁴⁰, Y. Xie⁶⁵,
M. Xu⁶⁵, Z. Xu⁴, Z. Yang³, Z. Yang⁶⁰, Y. Yao⁶¹, H. Yin⁶⁵, J. Yu⁶⁵, X. Yuan⁶¹,
O. Yushchenko³⁷, K.A. Zarebski⁴⁷, M. Zavertyaev^{11,c}, L. Zhang³, Y. Zhang⁷, A. Zhelezov¹²,
Y. Zheng⁶³, X. Zhu³, V. Zhukov³³, J.B. Zonneveld⁵², S. Zucchelli¹⁵.

¹Centro Brasileiro de Pesquisas Físicas (CBPF), Rio de Janeiro, Brazil

²Universidade Federal do Rio de Janeiro (UFRJ), Rio de Janeiro, Brazil

³Center for High Energy Physics, Tsinghua University, Beijing, China

⁴LAPP, Université Savoie Mont-Blanc, CNRS/IN2P3, Annecy-Le-Vieux, France

⁵Clermont Université, Université Blaise Pascal, CNRS/IN2P3, LPC, Clermont-Ferrand, France

⁶Aix Marseille Univ, CNRS/IN2P3, CPPM, Marseille, France

⁷LAL, Université Paris-Sud, CNRS/IN2P3, Orsay, France

⁸LPNHE, Université Pierre et Marie Curie, Université Paris Diderot, CNRS/IN2P3, Paris, France

⁹I. Physikalisches Institut, RWTH Aachen University, Aachen, Germany

¹⁰Fakultät Physik, Technische Universität Dortmund, Dortmund, Germany

¹¹Max-Planck-Institut für Kernphysik (MPIK), Heidelberg, Germany

¹²Physikalisches Institut, Ruprecht-Karls-Universität Heidelberg, Heidelberg, Germany

¹³School of Physics, University College Dublin, Dublin, Ireland

¹⁴Sezione INFN di Bari, Bari, Italy

- ¹⁵ *Sezione INFN di Bologna, Bologna, Italy*
- ¹⁶ *Sezione INFN di Cagliari, Cagliari, Italy*
- ¹⁷ *Universita e INFN, Ferrara, Ferrara, Italy*
- ¹⁸ *Sezione INFN di Firenze, Firenze, Italy*
- ¹⁹ *Laboratori Nazionali dell'INFN di Frascati, Frascati, Italy*
- ²⁰ *Sezione INFN di Genova, Genova, Italy*
- ²¹ *Universita e INFN, Milano-Bicocca, Milano, Italy*
- ²² *Sezione di Milano, Milano, Italy*
- ²³ *Sezione INFN di Padova, Padova, Italy*
- ²⁴ *Sezione INFN di Pisa, Pisa, Italy*
- ²⁵ *Sezione INFN di Roma Tor Vergata, Roma, Italy*
- ²⁶ *Sezione INFN di Roma La Sapienza, Roma, Italy*
- ²⁷ *Henryk Niewodniczanski Institute of Nuclear Physics Polish Academy of Sciences, Kraków, Poland*
- ²⁸ *AGH - University of Science and Technology, Faculty of Physics and Applied Computer Science, Kraków, Poland*
- ²⁹ *National Center for Nuclear Research (NCBJ), Warsaw, Poland*
- ³⁰ *Horia Hulubei National Institute of Physics and Nuclear Engineering, Bucharest-Magurele, Romania*
- ³¹ *Petersburg Nuclear Physics Institute (PNPI), Gatchina, Russia*
- ³² *Institute of Theoretical and Experimental Physics (ITEP), Moscow, Russia*
- ³³ *Institute of Nuclear Physics, Moscow State University (SINP MSU), Moscow, Russia*
- ³⁴ *Institute for Nuclear Research of the Russian Academy of Sciences (INR RAN), Moscow, Russia*
- ³⁵ *Yandex School of Data Analysis, Moscow, Russia*
- ³⁶ *Budker Institute of Nuclear Physics (SB RAS), Novosibirsk, Russia*
- ³⁷ *Institute for High Energy Physics (IHEP), Protvino, Russia*
- ³⁸ *ICCUB, Universitat de Barcelona, Barcelona, Spain*
- ³⁹ *Universidad de Santiago de Compostela, Santiago de Compostela, Spain*
- ⁴⁰ *European Organization for Nuclear Research (CERN), Geneva, Switzerland*
- ⁴¹ *Institute of Physics, Ecole Polytechnique Fédérale de Lausanne (EPFL), Lausanne, Switzerland*
- ⁴² *Physik-Institut, Universität Zürich, Zürich, Switzerland*
- ⁴³ *Nikhef National Institute for Subatomic Physics, Amsterdam, The Netherlands*
- ⁴⁴ *Nikhef National Institute for Subatomic Physics and VU University Amsterdam, Amsterdam, The Netherlands*
- ⁴⁵ *NSC Kharkiv Institute of Physics and Technology (NSC KIPT), Kharkiv, Ukraine*
- ⁴⁶ *Institute for Nuclear Research of the National Academy of Sciences (KINR), Kyiv, Ukraine*
- ⁴⁷ *University of Birmingham, Birmingham, United Kingdom*
- ⁴⁸ *H.H. Wills Physics Laboratory, University of Bristol, Bristol, United Kingdom*
- ⁴⁹ *Cavendish Laboratory, University of Cambridge, Cambridge, United Kingdom*
- ⁵⁰ *Department of Physics, University of Warwick, Coventry, United Kingdom*
- ⁵¹ *STFC Rutherford Appleton Laboratory, Didcot, United Kingdom*
- ⁵² *School of Physics and Astronomy, University of Edinburgh, Edinburgh, United Kingdom*
- ⁵³ *School of Physics and Astronomy, University of Glasgow, Glasgow, United Kingdom*
- ⁵⁴ *Oliver Lodge Laboratory, University of Liverpool, Liverpool, United Kingdom*
- ⁵⁵ *Imperial College London, London, United Kingdom*
- ⁵⁶ *School of Physics and Astronomy, University of Manchester, Manchester, United Kingdom*
- ⁵⁷ *Department of Physics, University of Oxford, Oxford, United Kingdom*
- ⁵⁸ *Massachusetts Institute of Technology, Cambridge, MA, United States*
- ⁵⁹ *University of Cincinnati, Cincinnati, OH, United States*
- ⁶⁰ *University of Maryland, College Park, MD, United States*
- ⁶¹ *Syracuse University, Syracuse, NY, United States*
- ⁶² *Pontifícia Universidade Católica do Rio de Janeiro (PUC-Rio), Rio de Janeiro, Brazil, associated to ²*
- ⁶³ *University of Chinese Academy of Sciences, Beijing, China, associated to ³*
- ⁶⁴ *School of Physics and Technology, Wuhan University, Wuhan, China, associated to ³*
- ⁶⁵ *Institute of Particle Physics, Central China Normal University, Wuhan, Hubei, China, associated to ³*
- ⁶⁶ *Departamento de Física, Universidad Nacional de Colombia, Bogota, Colombia, associated to ⁸*
- ⁶⁷ *Institut für Physik, Universität Rostock, Rostock, Germany, associated to ¹²*
- ⁶⁸ *National Research Centre Kurchatov Institute, Moscow, Russia, associated to ³²*

⁶⁹ *National Research Tomsk Polytechnic University, Tomsk, Russia, associated to* ³²

⁷⁰ *Instituto de Fisica Corpuscular, Centro Mixto Universidad de Valencia - CSIC, Valencia, Spain, associated to* ³⁸

⁷¹ *Van Swinderen Institute, University of Groningen, Groningen, The Netherlands, associated to* ⁴³

^a *Universidade Federal do Triângulo Mineiro (UFTM), Uberaba-MG, Brazil*

^b *Laboratoire Leprince-Ringuet, Palaiseau, France*

^c *P.N. Lebedev Physical Institute, Russian Academy of Science (LPI RAS), Moscow, Russia*

^d *Università di Bari, Bari, Italy*

^e *Università di Bologna, Bologna, Italy*

^f *Università di Cagliari, Cagliari, Italy*

^g *Università di Ferrara, Ferrara, Italy*

^h *Università di Genova, Genova, Italy*

ⁱ *Università di Milano Bicocca, Milano, Italy*

^j *Università di Roma Tor Vergata, Roma, Italy*

^k *Università di Roma La Sapienza, Roma, Italy*

^l *AGH - University of Science and Technology, Faculty of Computer Science, Electronics and Telecommunications, Kraków, Poland*

^m *LIFAELS, La Salle, Universitat Ramon Llull, Barcelona, Spain*

ⁿ *Hanoi University of Science, Hanoi, Viet Nam*

^o *Università di Padova, Padova, Italy*

^p *Università di Pisa, Pisa, Italy*

^q *Università degli Studi di Milano, Milano, Italy*

^r *Università di Urbino, Urbino, Italy*

^s *Università della Basilicata, Potenza, Italy*

^t *Scuola Normale Superiore, Pisa, Italy*

^u *Università di Modena e Reggio Emilia, Modena, Italy*

^v *Iligan Institute of Technology (IIT), Iligan, Philippines*

^w *Novosibirsk State University, Novosibirsk, Russia*

[†] *Deceased*